In-medium $NN \to N\Delta$ cross sections from constrained relativistic mean field models*

Ying Cui (崔莹)[1†] Enpei Liang (梁恩培)[1] Xinyu Wang (王馨钰)[1] Yuan Tian (田源)[1]
Zhuxia Li (李祝霞)[1] Yingxun Zhang (张英逊)[1,2‡]

[1]China Institute of Atomic Energy, Beijing 102413, China
[2]Guangxi Normal University, Guilin 541004, China

Abstract: The theoretical prediction on the in-medium $NN \to N\Delta$ cross sections based on a one-boson exchange model involves significant parameter uncertainties. In this work, we reduce these uncertainties by employing relativistic mean field models constrained by neutron star observations. Specifically, the range of the correction factors $R = \sigma^*_{NN\to N\Delta}/\sigma^{\rm free}_{NN\to N\Delta}$ is significantly narrowed at nuclear densities above saturation.

Keywords: in-medium $NN \to N\Delta$ cross sections, isospin-asymmetric nuclear matter, relativistic mean field models, equation of state

DOI: 10.1088/1674-1137/ae3072 **CSTR:** 32044.14.ChinesePhysicsC.50054101

The medium NN cross sections in transport mode simulations play a crucial role in intermediate-energy heavy ion collisions, as they significantly influence the predictions of reaction dynamics, collective flow, stopping power, and particle productions [1−9]. In transport model simulations, the in-medium $NN \to N\Delta$ cross sections are a critical component of the $\pi - N - \Delta$ loops, which can affect the pion multiplicity data. The π^-/π^+ ratio serves as a sensitive observable for probing the symmetry energy at suprasaturation density. The in-medium $NN \to N\Delta$ cross section ($\sigma^*_{NN\to N\Delta}$) is one of the important ingredients for reproducing the pion multiplicity data because it will directly influence the first Δ production, which can decay into nucleons and pions or rescatter with nucleons.

Many transport codes have adopted the free space $NN \to N\Delta$ cross section, *i.e.*, the $\sigma^{\rm free}_{NN\to N\Delta}$ obtained from Ref. [10], or phenomenological in-medium cross section, *i.e.*, $\sigma^*_{NN\to N\Delta} = R\sigma^{\rm free}_{NN\to N\Delta}$, in the collision integral of transport models [11]. Recent transport model comparison studies by the Transport Model Evaluation Project collaboration highlight the large model dependence in pion yields and the need for improved in-medium inputs [12−18]. Isospin independent microscopic approaches have been employed to investigate the in-medium $NN \to N\Delta$ cross sections in symmetric nuclear matter [19−25], where the medium correction factor R is the same for for all channels of the $NN \to N\Delta$ process. For isospin asymmetric nuclear matter, Li *et al*. studied the in-medium $NN \to N\Delta$ cross section without considering the mass distribution of Δ resonance and threshold effects by using the relativistic Boltzmann-Uehling-Uhlenbeck microscopic transport theory based on the closed time-path Green's function technique in Ref. [26].

In our previous work [27], the in-medium $NN \to N\Delta$ cross section $\sigma^*_{NN\to N\Delta}$ was analyzed by considering the threshold effect and the mass distribution of the Δ resonance in asymmetric nuclear matter. Further, the dependence of the medium correction factor R on the relativistic mean field (RMF) parameters was investigated in our previous study [28]. Using 3 RMF models, *i.e.*, NL$\rho\delta$ [29], DDMEδ [30], and DDRH$\rho\delta$ [31], our results showed that R increases with the slope parameter L when using δ parameter sets for a given isospin asymmetry. To better understand the influence of the δ meson on the in-medium $NN \to N\Delta$ cross sections, we compared calculations of R performed with and without δ-meson parameter sets in our subsequent work [32]. The results indicated that, when using parameter sets without the δ meson, the cross-section factors satisfy $R_{pp\to n\Delta^{++}} < R_{nn\to p\Delta^-}$ and $R_{NN\to N\Delta^+} < R_{NN\to N\Delta^0}$, whereas the opposite trend is observed when the δ meson is included.

Received 4 September 2025; Accepted 23 December 2025; Accepted manuscript online 24 December 2025

* This work was supported by the National Natural Science Foundation of China (12275359, 12375129, 11875323, 11961141003), the National Key R & D Program of China (2023YFA1606402), the Continuous Basic Scientific Research Project, the China Institute of Atomic Energy (YZ222407001301, YZ232604001601), the Leading Innovation Project of the CNNC (LC192209000701, LC202309000201), and the computing server SCATP in China Institute of Atomic Energy and Basic Research Special Zone

† E-mail: cuiying@ciae.ac.cn
‡ E-mail: zhyx@ciae.ac.cn

However, with more than 300 available mean field models, large uncertainty exists in these cross section results. Therefore, it is essential to reduce the in-medium $NN \to N\Delta$ cross sections, especially because they are increasingly vital for improving transport models — particularly in the context of pion production and for further constraining the symmetry energy at suprasaturation densities. In this paper, we provide reductions on the range of values for the in-medium $NN \to N\Delta$ cross sections in isospin asymmetric nuclear matter based on a selected subset of RMF models that have been constrained by neutron star observations, as discussed in our previous work [33].

The remainder of this paper is organized as follows. First, we briefly describe the properties of nuclear matter for different RMF models. Next, we discuss the constraints on the in-medium correction factor R for $NN \to N\Delta$ cross sections. Finally, we provide a summary of our findings.

For the calculation of the in-medium $NN \to N\Delta$cross section in nuclear matter, we employ a one-boson exchange model based on a relativistic Lagrangian that includes both nucleons and Δ. According to the structure of the Lagrangian, three types of RMF parameter sets are adopted to estimate the in-medium cross section, as discussed in Ref. [34]: (i) nonlinear models, (ii) density-dependent models, and (iii) point-coupling models. Detailed descriptions of these RMF models are provided in Appendix A. Subsequently, the in-medium $NN \to N\Delta$ cross sections are calculated based on the respective RMF Lagrangians, and the detailed derivation of the cross sections can be found in Appendix B.

We employ the same RMF Lagrangian to derive the nuclear matter properties, as detailed in Appendix A. Here, the binding energy per particle in asymmetric nuclear matter is expressed as follows:

$$E(\rho,\alpha) = \frac{\epsilon}{\rho} - m_N = E_0(\rho) + S(\rho)\alpha^2 + O(\alpha^4), \tag{1}$$

where $E_0(\rho) = E(\rho, \alpha = 0)$ is the binding energy in symmetric nuclear matter and $S(\rho)$ denotes the symmetry energy. Here, $\rho = \rho_n + \rho_p$ represents the total nuclear matter density, ϵ is the energy density, m_N is the nucleon mass, and $\alpha = (\rho_n - \rho_p)/(\rho_n + \rho_p)$ is the isospin asymmetry. The nuclear symmetry energy $S(\rho)$ is defined as

$$S(\rho) = \frac{1}{2}\frac{\partial^2 E(\rho,\alpha)}{\partial\alpha^2}\Big|_{\alpha=0}. \tag{2}$$

The symmetry energy is expanded in terms of $(\rho-\rho_0)/3\rho_0$:

$$S(\rho) = J + \frac{L}{3\rho_0}(\rho-\rho_0) + \frac{K_{sym}}{2}\frac{(\rho-\rho_0)^2}{\rho_0^2} + \cdots. \tag{3}$$

Here, $J = S(\rho_0)$ represents the symmetry energy at saturation density ρ_0. Parameters $L = 3\rho_0 \frac{\partial S}{\partial \rho}|_{\rho=\rho_0}$ and $K_{\rm sym} = 9\rho_0^2 \frac{\partial^2 S}{\partial \rho^2}|_{\rho=\rho_0}$ denote the slope and curvature of the symmetry energy at saturation density, respectively.

The coupling constants in RMF models are crucial for predicting the in-medium Δ production cross section as well as for determining the equation of state (EOS) of nuclear matter. To reduce the uncertainty in the in-medium $NN \to N\Delta$ cross sections, it is essential to select reasonable RMF models. In previous work [33], the EOS of nuclear matter was constrained using neutron star observations based on various RMF parameter sets. In this study, we calculate the in-medium $NN \to N\Delta$ cross sections using 180 RMF interaction sets, as described in Refs. [33, 35].

Furthermore, an important task is to evaluate the in-medium $NN \to N\Delta$ cross sections further using the selected RMF parameter sets that have been refined based on multiple neutron star observables from Refs. [33, 36, 37]. The final constrained RMF models are HC, FSUGZ03, IU-FSU, G2*, BSR8, BSR9, FA3, FZ3, and DD-F. The EOS parameters (incompressibility K_0, symmetry energy J, slope of symmetry energy L, and curvature of symmetry $K_{\rm sym}$) obtained with and without NS observations in this work are listed in Table 1. Additionally, the properties of nuclear matter and related parameters of all RMF models used here are detailed in Table C1 of Appendix C.

As a key step in calculating the in-medium cross sections (see Eq. (48) in Appendix B), it is first necessary to determine the Dirac effective masses of nucleons, effective pole masses of Δ resonances, and channel-dependent changes in vector self-energies. These quantities must be obtained based on the RMF parameter sets that have been constrained as described previously.

Figure 1 plots the effective mass of the nucleon (m_N^*/m_N) and effective pole masses of Δ $(m_{0,\Delta}^*/m_{0,\Delta})$ as functions of ρ/ρ_0 in symmetric nuclear matter. Except for NL$\rho\delta$A [29], NL$\rho\delta$B [29], DDMEδ [30], and DDRH$\rho\delta$

Table 1. Ranges of the EOS from the RMF models used.

	K_0/MeV	J/MeV	L/MeV	$K_{\rm sym}$/MeV
With neutron star constraint	216.87–297.75	29.70–31.62	29.08–69.86	-275.05–28.99
Without neutron star constraint	199.92–300.67	17.37–43.54	29.08–140.37	-275.05–398.27

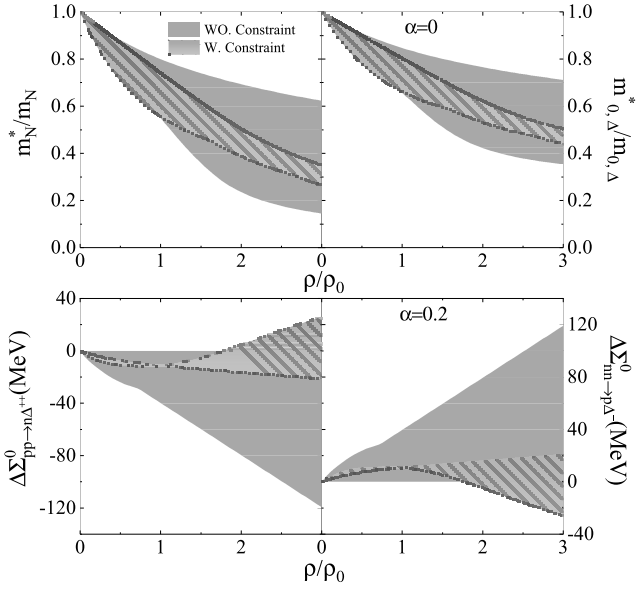

Fig. 1. Upper panels show the effective mass of the nucleon (m^*_N/m_N) and effective pole masses of Δ ($m^*_{0,\Delta}/m_{0,\Delta}$) in symmetric nuclear matter as functions of ρ/ρ_0. The lower panels display the changes in vector self-energies $\Delta\Sigma^0 pp \to n\Delta^{++}$ and $\Delta\Sigma^0 nn \to p\Delta^-$ in asymmetric nuclear matter with $\alpha = 0.2$. The pure gray areas represent the ranges of all considered RMF models, and the hatched areas indicate the subset constrained by neutron star observations. The constrained shaded band denotes the model-ensemble envelope—ranging from minimal to maximal values across all RMF interactions that pass the neutron-star filters—and is not a statistical confidence interval.

[31], all included constraint RMF models are without-δ models. Consequently, these models do not exhibit mass splitting between protons and neutrons (or among different Δ isospin states). Therefore, we only show the effective masses in symmetric nuclear matter.

Because most RMF models are adjusted to describe the nuclei and nuclear matter in the density region from near subsaturation density $\rho \approx 2/3\rho_0$(which represents the average value between the central and surface densities [38−43]) up to saturation density, significant uncertainties remain regarding RMF model properties — such as effective masses—at densities above ρ_0.

We can observe from the results in Fig. 1 that the uncertainty of the effective masses is reduced, *i.e.*, the range of $\Delta m^*_N = \dfrac{m^*_{N,\max} - m^*_{N,\min}}{m_N} = 0.196$ (corresponding to $m^*_N/m_N = 0.551 - 0.747$) at ρ_0, while $m^*_N/m_N = 0.677$–0.709 (corresponding to Δm^*_N=0.032), which are deduced at a 68% confidence level from only three types of momentum dependence of the optical potential model in Ref. [44]. Additionally, the range of $\Delta m^*_{0,\Delta}$ decreases, especially at the density above saturation density.

In our previous work [32], we observed that there remains a splitting among different channels of the in-medium $NN \to N\Delta$ cross sections in asymmetric nuclear matter. To illustrate this effect, we present the vector self-energy changes for two representative channels in asymmetric matter at $\alpha = 0.2$:

$$\Delta\Sigma^0_{pp\to n\Delta^{++}} = \Sigma^0_p + \Sigma^0_p - \Sigma^0_n - \Sigma^0_{\Delta^{++}},$$

and

$$\Delta\Sigma^0_{nn\to p\Delta^-} = \Sigma^0_n + \Sigma^0_n - \Sigma^0_p - \Sigma^0_{\Delta^-}.$$

These channels, $pp \to n\Delta^{++}$ and $nn \to p\Delta^-$, are highlighted because they are the main contributors to the $NN \to N\Delta$ processes.

The results indicate that the uncertainties in both the effective masses and vector self-energy changes are significantly reduced when using the constrained RMF models, especially at higher densities. Consequently, the uncertainties in the in-medium $NN \to N\Delta$ cross sections are expected to be diminished correspondingly.

Figure 2 displays the in-medium $pp \to n\Delta^{++}$ cross sections as a function of the total energy $\sqrt{s}$ in symmetric nuclear matter. The left panel compares the cross sections in free space and at saturation density, while the middle and right panels present the cross sections $\sigma^*_{pp\to n\Delta^{++}}$ at $\rho = 2\rho_0$ and $3\rho_0$, respectively. Compared with the unconstrained results, the constrained in-medium cross sections show a notably reduced spread, particularly at densities above ρ_0. This reduction in uncertainty of the in-medium cross section is consistent with the behaviors of the nucleon and Δ effective masses shown in Fig. 1. The in-medium $NN \to N\Delta$ cross section depends explicitly on the effective masses (m^*_N and $m^*_{0,\Delta}$) in symmetric nuclear matter (the channel-dependent vector self-energy changes $\Delta\Sigma^0$ should also be considered in asymmetric nuclear matter), which can be derived from Appendix B. Bulk "nuclear-matter properties" such as K_0, J, L, and $K_{\rm sym}$ do not enter the cross-section formula directly and are determined by RMF interactions. After applying neutron-star constraints, the surviving RMF sets develop similar trajectories of $m^*(\rho)$ and $\Delta\Sigma^0(\rho)$ at 2 to $3\rho_0$, which lead to the observed narrowing of in-medium cross sections, even though the spread in incompressibility of the same sets may remain sizable (*e.g.*, FA3 and FZ3).

As no isospin splitting of effective masses occurs in symmetric nuclear matter, the in-medium cross section for $nn \to p\Delta^-$ is identical to that for $pp \to n\Delta^{++}$. The cross sections for other channels can be obtained by applying the appropriate isospin Clebsch-Gordan coefficients, yielding values equal to $\frac{1}{3}\sigma^*_{pp\to n\Delta^{++}}$. Consequently, the ratio $R = \sigma^*_{NN\to N\Delta}/\sigma_{NN\to N\Delta}$ is the same for all channels of

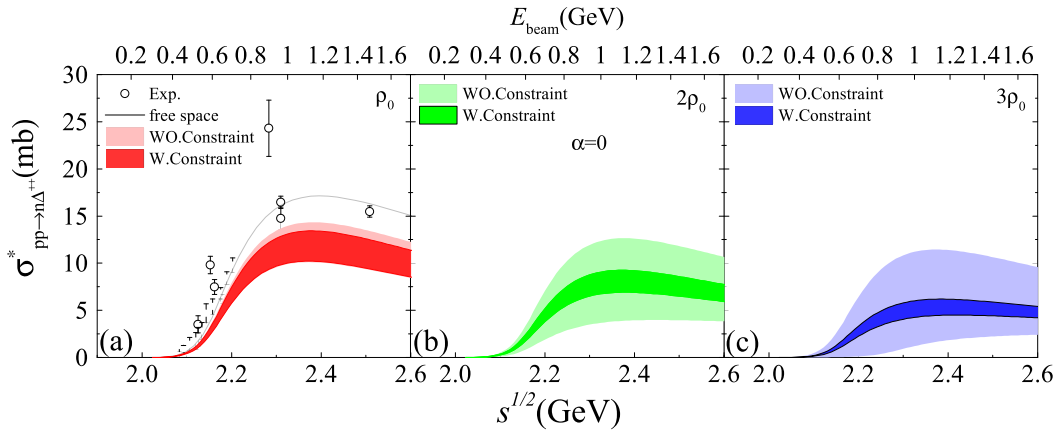

Fig. 2. (color online) In-medium $pp \to n\Delta^{++}$ cross section as function of $\sqrt{s}$ in symmetric nuclear matter. The left panel shows the cross section in free space and at ρ_0, while the middle and right panels present the results at $2\rho_0$ and $3\rho_0$, respectively. The experimental data are obtained from Ref. [45].

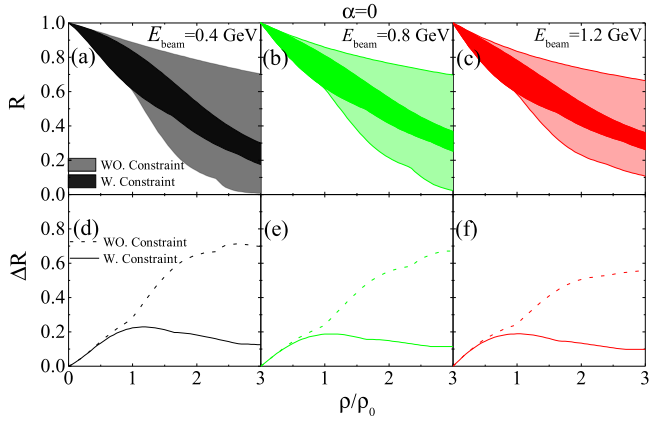

Fig. 3. (color online) Upper panels show R as a function of density ρ/ρ_0 at a beam energy of $E_{\rm beam} = 0.4$, 0.8, and 1.2 GeV in symmetric nuclear matter. The lower panels display the corresponding range ΔR.

$NN \to N\Delta$ in symmetric nuclear matter.

Figure 3 shows the medium correction factors R (top panels) and corresponding range $\Delta R = R_{\rm max} - R_{\rm min}$ (bottom panels) as a function of ρ/ρ_0 for beam energies $E_{\rm beam} = 0.4, 0.8$, and 1.2 GeV in symmetric nuclear matter. The unconstrained ΔR increases with the density, but once constraints are applied to the in-medium cross sections, the spread in R is notably reduced compared with the unconstrained results. For instance, at $E_{\rm beam} = 0.4$ GeV, ΔR decreases from 0.283 to 0.219 at ρ_0, from 0.648 to 0.182 at $2\rho_0$, and from 0.696 to 0.125 at $3\rho_0$. This reduction stems from the decreased uncertainty in the effective masses (see Fig. 1).

We use the $pp \to n\Delta^{++}$ and $nn \to p\Delta^-$ channels as examples to illustrate the in-medium cross sections in asymmetric nuclear matter. Figure 4 plots R for $pp \to n\Delta^{++}$ (panels (a), (b), and (c)) and $nn \to p\Delta^-$ (panels (d), (e), and (f)), the constrained median values $R_{\rm med}$ (panels (g), (h), and (i)), and the range ΔR (panels (j), (k), and (l)) as

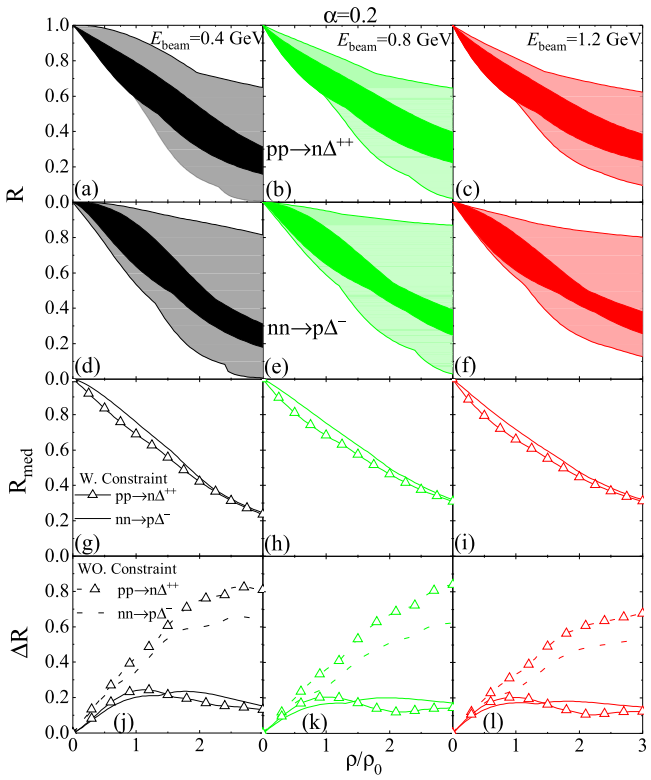

Fig. 4. (color online) The in-medium correction factor R for $pp \to n\Delta^{++}$ (panels (a), (b), and (c)) and $nn \to p\Delta^-$ (panels (d), (e), and (f)), the constraint median values of the correction factors $R_{\rm med}$ (panels (g), (h), and (i)), and ΔR (panels (j), (k), and (l)) as functions of density ρ/ρ_0 in asymmetric nuclear matter with $\alpha = 0.2$.

functions of ρ/ρ_0 in asymmetric nuclear matter with $\alpha = 0.2$ for $E_{\rm beam} = 0.4$, 0.8, and 1.2 GeV.

It is also evident that the constrained median values of the in-medium $NN \to N\Delta$ cross sections follow $R_{pp\to n\Delta^{++}} < R_{nn\to p\Delta^-}$, consistent with Ref. [32].

Furthermore, the constrained correction factors R in asymmetric nuclear matter are notably smaller than their unconstrained counterparts. For instance, at ρ_0, $\Delta R_{pp\to n\Delta^{++}}$ decreases from 0.347 to 0.202, while $\Delta R_{nn\to p\Delta^-}$ decreases from 0.427 to 0.238. Similar reductions are observed at $2\rho_0$ and $3\rho_0$. For example, at $2\rho_0$, $\Delta R_{pp\to n\Delta^{++}}$ decreases from 0.593 to 0.230, whereas $\Delta R_{nn\to p\Delta^-}$ decreases from 0.746 to 0.178. Overall, the restricted ΔR decreases by approximately 42%–44%, 61%–76%, and 76%–84% from $pp \to n\Delta^{++}$ to $nn \to p\Delta^-$ at at ρ_0, $2\rho_0$ and $3\rho_0$ respectively for $E_{\rm beam} = 0.4$ GeV, as well as for other beam energies.

Evaluating the in-medium $NN \to N\Delta$ cross sections in asymmetric nuclear matter is crucial for heavy-ion collision studies, as it provides a potential avenue for reducing uncertainties in the symmetry energy at suprasaturation densities. To facilitate their application in transport models, we present parameterizations of the constrained in-medium cross section correction factors R for all $NN \to N\Delta$ channels at beam energies $E_{\rm beam} = 0.4$, $0.6, 0.8, 1.0$, and 1.2 GeV, in both symmetric and asymmetric nuclear matter.

In summary, we present the evaluated the in-medium $NN \to N\Delta$ cross sections derived from RMF parameter sets constrained by neutron star observations [33]. Compared with the unconstrained results, our findings show that the ranges of $\sigma^*_{NN\to N\Delta}$ are significantly reduced over the density range $0 < \rho \le 3\rho_0$ for beam energies of $E_{\rm beam} = 0.4, 0.8$, and 1.2 GeV in both symmetric and asymmetric nuclear matter, especially at densities above ρ_0. For completeness, the parameterized forms of the in-medium $NN \to N\Delta$ cross-section corrections are provided in the supplemental material.

We believe that the constrained in-medium cross sections will help to reduce the uncertainties of information on the symmetry energy at high densities by facilitating them in the prediction of pion observables in QMD models for simulating heavy-ion collision experiments, such as those performed by the HADES (Au+Au) [46] and MSU (Sn+Sn) [15]. However, matter created in heavy ion collisions is hot and in a non-equilibrium state, which implies that the in-medium $NN \to N\Delta$ cross section depends on the temperature. Prior work has explored the temperature dependence of in-medium nucleon-nucleon scattering cross sections (see Ref. [47]), reporting a possible enhancement at a finite temperature relative to the cold matter case. The explicit temperature dependence of in-medium $NN \to N\Delta$ cross sections has rarely been discussed, and we will investigate it in future work.

APPENDIX A: RELATIVISTIC MEAN FIELD

In this paper, we ignore the Fock term in the relativistic mean field, where the models are all Hartree RMF model sets.

1. Nonlinear RMF

The Lagrangians in the nonlinear RMF model are

$$\mathcal{L}_{NL} = \mathcal{L}_F + \mathcal{L}_I, \tag{A1}$$

where $\mathcal{L}_F$ is

$$\begin{aligned}\mathcal{L}_F =& \bar{\Psi}[\mathrm{i}\gamma_\mu\partial^\mu - m_N]\Psi + \bar{\Delta}_\lambda[\mathrm{i}\gamma_\mu\partial^\mu - m_\Delta]\Delta^\lambda \\ &+ \frac{1}{2}\left(\partial_\mu\boldsymbol{\pi}\partial^\mu\boldsymbol{\pi} - m_\pi^2\boldsymbol{\pi}^2\right) + \frac{1}{2}\partial_\mu\sigma\partial^\mu\sigma - \frac{1}{2}m_\sigma^2\sigma^2 - U(\sigma) \\ &- \frac{1}{4}\omega_{\mu\nu}\omega^{\mu\nu} + \frac{1}{2}m_\omega^2\omega_\mu\omega^\mu + \frac{1}{4}\zeta^4(\omega_\mu\omega^\mu)^2 \\ &- \frac{1}{4}\boldsymbol{\rho}_{\mu\nu}\boldsymbol{\rho}^{\mu\nu} + \frac{1}{2}m_\rho^2\boldsymbol{\rho}_\mu\boldsymbol{\rho}^\mu + \frac{1}{2}\left(\partial_\mu\boldsymbol{\delta}\partial^\mu\boldsymbol{\delta} - m_\delta^2\boldsymbol{\delta}^2\right) \\ &+ g_\sigma g_\omega^2\sigma\omega_\mu\omega^\mu(\alpha_1 + \frac{1}{2}\alpha_1' g_\sigma) + g_\sigma g_\rho^2\sigma\boldsymbol{\rho}_\mu\boldsymbol{\rho}^\mu(\alpha_2 + \frac{1}{2}\alpha_2' g_\sigma) \\ &+ \frac{1}{2}\alpha_3' g_\omega^2 g_\rho^2\omega_\mu\omega^\mu\boldsymbol{\rho}_\mu\boldsymbol{\rho}^\mu\,.\end{aligned} \tag{A2}$$

$\mathcal{L}_I$ is the interaction part:

$$\begin{aligned}\mathcal{L}_I =& g_{\sigma NN}\bar{\Psi}\Psi\sigma - g_{\omega NN}\bar{\Psi}\gamma_\mu\Psi\omega^\mu - g_{\rho NN}\bar{\Psi}\gamma_\mu\boldsymbol{\tau}\cdot\Psi\boldsymbol{\rho}^\mu \\ &- \frac{f_{\pi NN}}{m_\pi}\bar{\Psi}\gamma_\mu\gamma_5\boldsymbol{\tau}\cdot\Psi\partial^\mu\boldsymbol{\pi} + g_{\delta NN}\bar{\Psi}\boldsymbol{\tau}\cdot\Psi\boldsymbol{\delta} \\ &+ g_{\sigma\Delta\Delta}\bar{\Delta}_\mu\Delta^\mu\sigma - g_{\omega\Delta\Delta}\bar{\Delta}_\mu\gamma_\nu\Delta^\mu\omega^\nu \\ &- g_{\rho\Delta\Delta}\bar{\Delta}_\mu\gamma_\nu\mathbf{T}\cdot\Delta^\mu\boldsymbol{\rho}^\nu + \frac{g_{\pi\Delta\Delta}}{m_\pi}\bar{\Delta}_\mu\gamma_\nu\gamma_5\mathbf{T}\cdot\Delta^\mu\partial^\nu\boldsymbol{\pi} \\ &+ g_{\delta\Delta\Delta}\bar{\Delta}_\mu\mathbf{T}\cdot\Delta^\mu\boldsymbol{\delta} + \frac{g_{\pi N\Delta}}{m_\pi}\bar{\Delta}_\mu\mathcal{T}\cdot\Psi\partial^\mu\boldsymbol{\pi} \\ &+ \frac{\mathrm{i}g_{\rho N\Delta}}{m_\rho}\bar{\Delta}_\mu\gamma_\nu\gamma_5\mathcal{T}\cdot\Psi(\partial^\nu\boldsymbol{\rho}^\mu - \partial^\mu\boldsymbol{\rho}^\nu) + h.c.\end{aligned} \tag{A3}$$

In Eq. (A2), $\omega_{\mu\nu}$ and $\boldsymbol{\rho}_{\mu\nu}$ are defined as $\partial_\mu\omega_\nu - \partial_\nu\omega_\mu$ and $\partial_\mu\boldsymbol{\rho}_\nu - \partial_\nu\boldsymbol{\rho}_\mu$, respectively. The nonlinear potential of the σ field is determined by $U(\sigma) = \frac{1}{3}g_2\sigma^3 + \frac{1}{4}g_3\sigma^4$. Here, $\boldsymbol{\tau}$ and $\mathbf{T}$ are the isospin matrices for the nucleon and Δ [48, 49], respectively, while $\mathcal{T}$ is the isospin transition matrix between the isospin 1/2 and 3/2 fields [10].

In uniform rest nuclear matter, the effective momentum can be written as $\mathbf{p}_i^* = \mathbf{p}_i$ because the spatial components of the vector field vanish, *i.e.*, $\boldsymbol{\Sigma} = 0$. Thus, in the mean field approach, the effective energy is expressed as:

$$p_i^{*0} = p_i^0 - \Sigma_i^0, \tag{A4}$$

and the effective masses of the nucleon and Δ are

$$m_i^* = m_i + \Sigma_i^S, \tag{A5}$$

where Σ_i^0 and Σ_i^S represent the vector and scalar self-energies, respectively, for the RMF parameter sets.

The vector and scalar potentials in the nonlinear RMF model are expressed as

$$\Sigma^0_{i,NL} = g_\omega\bar{\omega}^0 + g_\rho t_{3,i}\bar{\rho}^0_3, \tag{A6}$$

$$\Sigma^S_{i,NL} = -g_\sigma\bar{\sigma} - g_\delta t_{3,i}\bar{\delta}_3, \tag{A7}$$

where $t_{3,i}$ represents the third component of the isospin of the nucleon and Δ, with the following values: $t_{3,n} = -1$, $t_{3,p} = 1$, $t_{3,\Delta^{++}} = 1$, $t_{3,\Delta^+} = 1/3$, $t_{3,\Delta^0} = -1/3$, and $t_{3,\Delta^-} = -1$. $\bar{\omega}^0$, $\bar{\rho}^0_3$, $\bar{\sigma}$, and $\bar{\delta}_3$ denote the expectation values of the meson field in the mean-field approximation. In the RMF model, the equations of motion for the mesons are

$$\begin{aligned} m^2\bar{\sigma} = {} & g_\sigma\rho_s - g_2\bar{\sigma}^2 - g_3\bar{\sigma}^3 + g_\sigma g_\omega^2(\bar{\omega}^0)^2(\alpha_1 + \alpha_1' g_\sigma\bar{\sigma}) \\ & + g_\sigma g_\rho^2(\bar{\rho}^0_3)^2(\alpha_2 + \alpha_2' g_\sigma\bar{\sigma}), \end{aligned} \tag{A8}$$

$$\begin{aligned} m_\omega^2\bar{\omega}^0 = {} & g_\omega\rho - \zeta g_\omega^4(\bar{\omega}^0)^3 - g_\sigma g_\omega^2\bar{\sigma}\bar{\omega}^0(2\alpha_1 + \alpha_1' g_\sigma\bar{\sigma}) \\ & - \alpha_3' g_\omega^2 g_\rho^2(\bar{\rho}^0_3)^2\bar{\omega}^0, \end{aligned} \tag{A9}$$

$$\begin{aligned} m_\rho^2\bar{\rho}^0_3 = {} & g_\rho\rho_3 - g_\sigma g_\rho^2\bar{\sigma}\bar{\rho}^0_3(2\alpha_2 + \alpha_2' g_\sigma\bar{\sigma}) \\ & - \alpha_3' g_\omega^2 g_\rho^2\bar{\rho}^0_3(\bar{\omega}^0)^2, \end{aligned} \tag{A10}$$

$$m_\delta^2\bar{\delta}_3 = g_\delta\rho_{s3}. \tag{A11}$$

The nucleon densities (assuming no Δ density) are

$$\rho_s = \langle\bar{\Psi}\Psi\rangle = \rho_{sn} + \rho_{sp}, \tag{A12}$$

$$\rho = \langle\bar{\Psi}\gamma^0\Psi\rangle = \rho_n + \rho_p, \tag{A13}$$

$$\rho_{s3} = \langle\bar{\Psi}\tau_3\Psi\rangle = \rho_{sp} - \rho_{sn}, \tag{A14}$$

$$\rho_3 = \langle\bar{\Psi}\gamma^0\tau_3\Psi\rangle = \rho_p - \rho_n. \tag{A15}$$

With Fermi momenta $k_{F,i}$ for $i = n$ or p, the scalar and vector densities are

$$\begin{aligned} \rho_{si} &= \frac{C(i)}{(2\pi)^3}\int_{k<k_{Fi}} \mathrm{d}^3\mathbf{k}\frac{m_i^*}{\sqrt{k^2 + m_i^{*2}}} \\ &= \frac{m_i^*}{2\pi^2}\left[k_{Fi}E^*_{Fi} - m_i^{*2}\ln\frac{k_{Fi} + E^*_{Fi}}{m_i^*}\right], \end{aligned} \tag{A16}$$

$$\rho_i = \frac{C(i)}{(2\pi)^3}\int_{k<k_{Fi}} \mathrm{d}^3\mathbf{k} = \frac{k_{Fi}^3}{3\pi^2}, \tag{A17}$$

where the degeneracy factor $C(i = n, p) = 2$, and $E^*_{Fi} = \sqrt{k_{Fi}^2 + m_i^{2*}}$ is the Fermi energy of the neutrons and protons.

The eigenvalues of the neutron and proton from the Dirac equation are

$$e_n = g_\omega\bar{\omega}^0 - g_\rho\bar{\rho}^0_3 + \sqrt{k_n^{2*} + m_n^{*2}}, \tag{A18}$$

$$e_p = g_\omega\bar{\omega}^0 + g_\rho\bar{\rho}^0_3 + \sqrt{k_p^{2*} + m_p^{*2}}. \tag{A19}$$

The expressions for the energy density and pressure are obtained from the given Lagrangian using the energy momentum tensor relation:

$$T^{\mu\nu} = \sum_i \frac{\partial\mathcal{L}}{\partial(\partial_\mu\phi_i)}\partial^\nu\phi_i - g^{\mu\nu}\mathcal{L}, \tag{A20}$$

where ϕ_i runs over all possible fields. The energy density ϵ and pressure P can be obtained from the energy-momentum tensor:

$$\begin{aligned} \epsilon_{NL} = \langle T^{00}\rangle = {} & \frac{1}{2}m_\sigma^2\bar{\sigma}^2 + \frac{1}{3}g_2\bar{\sigma}^3 + \frac{1}{4}g_3\bar{\sigma}^4 - \frac{1}{2}m_\omega^2(\bar{\omega}^0)^2 \\ & - \frac{\zeta}{4}g_\omega^4(\bar{\omega}^0)^4 + g_\omega\bar{\omega}^0\rho - \frac{1}{2}m_\rho^2(\bar{\rho}^0_3)^2 + g_\rho\bar{\rho}^0_3\rho_3 \\ & + \frac{1}{2}m_\delta^2\bar{\delta}_3^2 - g_\sigma g_\omega^2\bar{\sigma}(\bar{\omega}^0)^2(\alpha_1 + \frac{1}{2}\alpha_1' g_\sigma\bar{\sigma}) \\ & - g_\sigma g_\rho^2\bar{\sigma}(\bar{\rho}^0_3)^2(\alpha_2 + \frac{1}{2}\alpha_2' g_\sigma\bar{\sigma}) - \frac{1}{2}\alpha_3' g_\omega^2 g_\rho^2(\bar{\rho}^0_3)^2(\bar{\omega}^0)^2 \\ & + \frac{1}{4}[3E^*_{Fn}\rho_n + m_n^*\rho_{sn}] + \frac{1}{4}[3E^*_{Fp}\rho_p + m_p^*\rho_{sp}], \end{aligned} \tag{A21}$$

and

$$\begin{aligned} P_{NL} = {} & \frac{1}{3}\sum_{i=1}^{3}\langle T^{ii}\rangle = -\frac{1}{2}m_\sigma^2\bar{\sigma}^2 - \frac{1}{3}g_2\bar{\sigma}^3 - \frac{1}{4}g_3\bar{\sigma}^4 \\ & + \frac{1}{2}m_\omega^2(\bar{\omega}^0)^2 + \frac{\zeta}{4}g_\omega^4(\bar{\omega}^0)^4 + \frac{1}{2}m_\rho^2(\bar{\rho}^0_3)^2 \\ & - \frac{1}{2}m_\delta^2\bar{\delta}_3^2 + g_\sigma g_\omega^2\bar{\sigma}(\bar{\omega}^0)^2(\alpha_1 + \frac{1}{2}\alpha_1' g_\sigma\bar{\sigma}) \\ & + g_\sigma g_\rho^2\bar{\sigma}(\bar{\rho}^0_3)^2(\alpha_2 + \frac{1}{2}\alpha_2' g_\sigma\bar{\sigma}) + \frac{1}{2}\alpha_3' g_\omega^2 g_\rho^2(\bar{\rho}^0_3)^2(\bar{\omega}^0)^2 \\ & + \frac{1}{4}[E^*_{Fn}\rho_n - m_n^*\rho_{sn}] + \frac{1}{4}[E^*_{Fp}\rho_p - m_p^*\rho_{sp}]. \end{aligned} \tag{A22}$$

The same calculations for the density-dependence and point-coupling models can be found in Refs. [30, 31, 50−52].

For symmetric nuclear matter, $m_n^* = m_p^* = m_N^*$ because $\bar{\delta}_3$ vanishes.

The expressions for the symmetry energy and slope of the symmetry energy L for nonlinear RMF models are

$$S(\rho)_{NL} = \frac{k_F^2}{6E_F^*} + \frac{1}{2}\rho\frac{g_\rho^2}{m_\rho^{*2}} - \frac{1}{2}\rho\left(\frac{\frac{g_\delta^2}{m_\delta^2}m_N^{*2}}{E_F^{*2}\left[1+\frac{g_\delta^2}{m_\delta^2}A(\rho,m_N^*)\right]}\right), \tag{A23}$$

where $m_\rho^{*2} = m_\rho^2 + g_\sigma g_\rho^2\bar{\sigma}(2\alpha_2 + \alpha_2' g_\sigma\bar{\sigma}) + \alpha_3' g_\omega^2 g_\rho^2(\bar{\omega}^0)^2$, and

$$A(\rho,m_N^*) = 3\left(\frac{\rho_s}{m_N^*} - \frac{\rho}{E_F^*}\right). \tag{A24}$$

$$\begin{aligned} L_{NL} = {} & \frac{k_F^2}{3E_F^*}\left(1-\frac{k_F^2}{2E_F^{*2}} - \frac{k_F^3 m_N^*}{E_F^{*2}\pi^2}\frac{\partial m_N^*}{\partial\rho}\right) \\ & + \frac{3g_\rho^2}{2m_\rho^{*2}}\rho\left(1-\frac{1}{m_\rho^{*2}}\frac{\partial m_\rho^{*2}}{\partial\rho}\rho\right) \\ & - \frac{1}{2}\rho\left(\frac{\frac{g_\delta^2}{m_\delta^2}m_N^{*2}}{E_F^{*2}\left[1+\frac{g_\delta^2}{m_\delta^2}A(\rho,m_N^*)\right]}\right) \\ & \times\left\{3-\frac{2k_F^2}{E_F^{*2}} + 6\left(1-\frac{m_N^{*2}}{E_F^{*2}}\right)\frac{\rho}{m_N^*}\frac{\partial m_N^*}{\partial\rho} \right. \\ & - 3\frac{g_\delta^2}{m_\delta^2}\frac{1}{1+\frac{g_\delta^2}{m_\delta^2}A}\left[2A\left(\frac{\rho}{m_N^*}\frac{\partial m_N^*}{\partial\rho}\right)\right. \\ & \left.\left. + \rho\frac{k_F^2}{E_F^{*3}}\left(1-3\frac{\rho}{m_N^*}\frac{\partial m_N^*}{\partial\rho}\right)\right]\right\}. \end{aligned} \tag{A25}$$

2. Density dependence RMF

The Lagrangian density of the density dependence model is

$$\mathcal{L}_{DD} = \mathcal{L}_I + \mathcal{L}_F, \tag{A26}$$

where $\mathcal{L}_F$ is

$$\begin{aligned} \mathcal{L}_F = {} & \bar{\Psi}[\mathrm{i}\gamma_\mu\partial^\mu - m_N]\Psi + \bar{\Delta}_\lambda[\mathrm{i}\gamma_\mu\partial^\mu - m_\Delta]\Delta^\lambda \\ & + \frac{1}{2}\left(\partial_\mu\sigma\partial^\mu\sigma - m_\sigma^2\sigma^2\right) - \frac{1}{4}\omega_{\mu\nu}\omega^{\mu\nu} + \frac{1}{2}m_\omega^2\omega_\mu\omega^\mu \\ & + \frac{1}{2}\left(\partial_\mu\boldsymbol{\pi}\partial^\mu\boldsymbol{\pi} - m_\pi^2\boldsymbol{\pi}^2\right) - \frac{1}{4}\boldsymbol{\rho}_{\mu\nu}\boldsymbol{\rho}^{\mu\nu} + \frac{1}{2}m_\rho^2\boldsymbol{\rho}_\mu\boldsymbol{\rho}^\mu \\ & + \frac{1}{2}\left(\partial_\mu\boldsymbol{\delta}\partial^\mu\boldsymbol{\delta} - m_\delta^2\boldsymbol{\delta}^2\right), \end{aligned} \tag{A27}$$

and $\mathcal{L}_I$ is

$$\begin{aligned} \mathcal{L}_I = {} & \mathcal{L}_{NN} + \mathcal{L}_{\Delta\Delta} + \mathcal{L}_{N\Delta} \\ = {} & \Gamma_\sigma(\rho)\bar{\Psi}\Psi\sigma - \Gamma_\omega(\rho)\bar{\Psi}\gamma_\mu\Psi\omega^\mu - \Gamma_\rho(\rho)\bar{\Psi}\gamma_\mu\boldsymbol{\tau}\cdot\Psi\boldsymbol{\rho}^\mu \\ & + \frac{g_{\pi NN}}{m_\pi}\bar{\Psi}\gamma_\mu\gamma_5\boldsymbol{\tau}\cdot\Psi\partial^\mu\boldsymbol{\pi} + \Gamma_\delta(\rho)\bar{\Psi}\boldsymbol{\tau}\cdot\Psi\boldsymbol{\delta} \\ & + \Gamma_\sigma(\rho)\bar{\Delta}_\mu\Delta^\mu\sigma - \Gamma_\omega(\rho)\bar{\Delta}_\mu\gamma_\nu\Delta^\mu\omega^\nu \\ & - \Gamma_\rho(\rho)\bar{\Delta}_\mu\gamma_\nu\mathbf{T}\cdot\Delta^\mu\boldsymbol{\rho}^\nu + \frac{g_{\pi\Delta\Delta}}{m_\pi}\bar{\Delta}_\mu\gamma_\nu\gamma_5\mathbf{T}\cdot\Delta^\mu\partial^\nu\boldsymbol{\pi} \\ & + \Gamma_\delta(\rho)\bar{\Delta}_\mu\mathbf{T}\cdot\Delta^\mu\boldsymbol{\delta} + \frac{g_{\pi N\Delta}}{m_\pi}\bar{\Delta}_\mu\mathcal{T}\cdot\Psi\partial^\mu\boldsymbol{\pi} \\ & + \frac{\mathrm{i}g_{\rho N\Delta}}{m_\rho}\bar{\Delta}_\mu\gamma_\nu\gamma_5\mathcal{T}\cdot\Psi(\partial^\nu\boldsymbol{\rho}^\mu - \partial^\mu\boldsymbol{\rho}^\nu) + h.c. \end{aligned} \tag{A28}$$

The vector and scalar potentials can be expressed as

$$\Sigma_{i,DD}^0 = \Gamma_\omega\bar{\omega}^0 + \Gamma_\rho t_{3,i}\bar{\rho}_3^0 + \Sigma^r, \tag{A29}$$

$$\Sigma_{i,DD}^S = -\Gamma_\sigma\bar{\sigma} - \Gamma_\delta t_{3,i}\bar{\delta}_3. \tag{A30}$$

Here, Σ^r is the rearrangement term of the vector self-energy, which is expressed as

$$\Sigma^r = \frac{\partial\Gamma_\omega}{\rho}\bar{\omega}^0\rho + \frac{\partial\Gamma_\rho}{\partial\rho}\bar{\rho}_3^0\rho_3 - \frac{\partial\Gamma_\sigma}{\rho}\bar{\sigma}\rho_s - \frac{\partial\Gamma_\delta}{\rho}\bar{\delta}_3\rho_{s3}. \tag{A31}$$

The expressions of for the symmetry energy and slope of the symmetry energy L for density-dependent RMF models are

$$S(\rho)_{DD} = \frac{k_F^2}{6E_F^*} + \frac{1}{2}\rho\frac{\Gamma_\rho^2}{m_\rho^2} - \frac{1}{2}\rho\times\left(\frac{\frac{\Gamma_\delta^2}{m_\delta^2}m_N^{*2}}{E_F^{*2}\left[1+\frac{\Gamma_\delta^2}{m_\delta^2}A(\rho,m_N^*)\right]}\right), \tag{A32}$$

$$\begin{aligned} L_{DD} = {} & \frac{k_F^2}{3E_F^*}\left(1-\frac{k_F^2}{2E_F^{*2}} - \frac{k_F^3 m_N^*}{E_F^{*2}\pi^2}\frac{\partial m_N^*}{\partial\rho}\right) \\ & + \frac{3\Gamma_\rho^2}{2m_\rho^2}\rho\left(1+6\frac{\rho}{\Gamma_\rho}\frac{\partial\Gamma_\rho}{\partial\rho}\right) \\ & - \frac{1}{2}\rho\left(\frac{\frac{\Gamma_\delta^2}{m_\delta^2}m_N^{*2}}{E_F^{*2}\left[1+\frac{\Gamma_\delta^2}{m_\delta^2}A(\rho,m_N^*)\right]}\right) \\ & \times\left\{3+6\frac{\rho}{\Gamma_\delta}\frac{\partial\Gamma_\delta}{\partial\rho} - \frac{2k_F^2}{E_F^{*2}} + 6\left(1-\frac{m_N^{*2}}{E_F^{*2}}\right)\frac{\rho}{m_N^*}\frac{\partial m_N^*}{\partial\rho}\right. \end{aligned}$$

$$-3\frac{\Gamma_\delta^2}{m_\delta^2}\frac{1}{1+\frac{\Gamma_\delta^2}{m_\delta^2}A}\left[2A\left(\frac{\rho}{\Gamma_\delta}\frac{\partial\Gamma_\delta}{\partial\rho}+\frac{\rho}{m_N^*}\frac{\partial m_N^*}{\partial\rho}\right)+\rho\frac{k_F^2}{E_F^{*3}}\left(1-3\frac{\rho}{m_N^*}\frac{\partial m_N^*}{\partial\rho}\right)\right]\Bigg\}. \tag{A33}$$

3. Point coupling model

The Lagrangian density of the point coupling mean field model is

$$\mathcal{L}_{PC}=\mathcal{L}_F+\mathcal{L}_I, \tag{A34}$$

where $\mathcal{L}_F$ is

$$\mathcal{L}_F=\bar{\Psi}[\mathrm{i}\gamma_\mu\partial^\mu-m_N]\Psi+\bar{\Delta}_\lambda[\mathrm{i}\gamma_\mu\partial^\mu-m_\Delta]\Delta^\lambda, \tag{A35}$$

and $\mathcal{L}_I$ is

$$\begin{aligned}\mathcal{L}_I=&-\frac{\alpha_S}{2}\left(\bar{\Psi}\Psi\right)^2-\frac{\alpha_V}{2}\left(\bar{\Psi}\gamma_\mu\Psi\right)\left(\bar{\Psi}\gamma^\mu\Psi\right)\\&-\frac{\alpha_{TV}}{2}\left(\bar{\Psi}\gamma_\mu\boldsymbol{\tau}\Psi\right)\cdot\left(\bar{\Psi}\gamma^\mu\boldsymbol{\tau}\Psi\right)\\&-\frac{f_{\pi NN}}{m_\pi}\left(\bar{\Psi}\gamma_\mu\gamma_5\boldsymbol{\tau}\Psi\right)\cdot\partial^\mu\left(\bar{\Psi}\gamma_5\boldsymbol{\tau}\Psi\right)\\&-\frac{\alpha_{TS}}{2}\left(\bar{\Psi}\boldsymbol{\tau}\Psi\right)\cdot\left(\bar{\Psi}\boldsymbol{\tau}\Psi\right)\\&-\frac{\beta_S}{3}\left(\bar{\Psi}\Psi\right)^3-\frac{\gamma_S}{4}\left(\bar{\Psi}\Psi\right)^4-\frac{\gamma_V}{4}\left(\bar{\Psi}\gamma_\mu\Psi\bar{\Psi}\gamma^\mu\Psi\right)^2\\&-\frac{\alpha_{TV}}{4}\left(\bar{\Psi}\gamma_\mu\boldsymbol{\tau}\Psi\cdot\bar{\Psi}\gamma^\mu\boldsymbol{\tau}\Psi\right)^2\\&+[\eta_1+\eta_2\left(\bar{\Psi}\Psi\right)]\left(\bar{\Psi}\Psi\right)\left(\bar{\Psi}\gamma_\mu\Psi\right)\left(\bar{\Psi}\gamma^\mu\Psi\right)\\&-\eta_3\left(\bar{\Psi}\Psi\right)\left(\bar{\Psi}\gamma_\mu\boldsymbol{\tau}\Psi\right)\cdot\left(\bar{\Psi}\gamma^\mu\boldsymbol{\tau}\Psi\right)\\&-\frac{\alpha_S}{2}[\left(\bar{\Delta}_\mu\Delta^\mu\right)\left(\bar{\Psi}\Psi\right)+\left(\bar{\Psi}\Psi\right)\left(\bar{\Delta}_\mu\Delta^\mu\right)]\\&-\frac{\alpha_V}{2}[\left(\bar{\Delta}_\mu\gamma_\nu\Delta^\mu\right)\left(\bar{\Psi}\gamma^\nu\Psi\right)+\left(\bar{\Psi}\gamma_\nu\Psi\right)\left(\bar{\Delta}_\mu\gamma^\nu\Delta^\mu\right)]\\&-\frac{\alpha_{TV}}{2}[\left(\bar{\Delta}_\mu\gamma_\nu\mathbf{T}\Delta^\mu\right)\cdot\left(\bar{\Psi}\gamma^\nu\boldsymbol{\tau}\Psi\right)\\&+\left(\bar{\Psi}\gamma_\nu\boldsymbol{\tau}\Psi\right)\cdot\left(\bar{\Delta}_\mu\gamma^\nu\mathbf{T}\Delta^\mu\right)]\\&-\frac{\alpha_{TS}}{2}[\left(\bar{\Delta}_\mu\mathbf{T}\Delta^\mu\right)\cdot\left(\bar{\Psi}\boldsymbol{\tau}\Psi\right)+\left(\bar{\Psi}\boldsymbol{\tau}\Psi\right)\cdot\left(\bar{\Delta}_\mu\mathbf{T}\Delta^\mu\right)]\\&-\frac{\beta_S}{3}[\left(\bar{\Delta}_\mu\Delta^\mu\right)\left(\bar{\Psi}\Psi\right)^2+\left(\bar{\Psi}\Psi\right)\left(\bar{\Delta}_\mu\Delta^\mu\right)\left(\bar{\Psi}\Psi\right)\\&+\left(\bar{\Psi}\Psi\right)^2\left(\bar{\Delta}_\mu\Delta^\mu\right)]\\&-\frac{\gamma_S}{4}[\left(\bar{\Delta}_\mu\Delta^\mu\right)\left(\bar{\Psi}\Psi\right)^3+\left(\bar{\Psi}\Psi\right)\left(\bar{\Delta}_\mu\Delta^\mu\right)\left(\bar{\Psi}\Psi\right)^2\\&+\left(\bar{\Psi}\Psi\right)^2\left(\bar{\Delta}_\mu\Delta^\mu\right)\left(\bar{\Psi}\Psi\right)+\left(\bar{\Psi}\Psi\right)^3\left(\bar{\Delta}_\mu\Delta^\mu\right)]\\&-\frac{\gamma_V}{4}[\left(\bar{\Delta}_\mu\gamma_\nu\Delta^\mu\bar{\Psi}\gamma^\nu\Psi\right)\left(\bar{\Psi}\gamma_\nu\Psi\bar{\Psi}\gamma^\nu\Psi\right)\\&+\left(\bar{\Psi}\gamma_\nu\Psi\bar{\Delta}_\mu\gamma^\nu\Delta^\mu\right)\left(\bar{\Psi}\gamma_\nu\Psi\bar{\Psi}\gamma^\nu\Psi\right)\\&+\left(\bar{\Psi}\gamma_\nu\Psi\bar{\Psi}\gamma^\nu\Psi\right)\left(\bar{\Psi}\gamma_\nu\Psi\bar{\Delta}_\mu\gamma^\nu\Delta^\mu\right)\\&+\left(\bar{\Psi}\gamma_\nu\Psi\bar{\Psi}\gamma^\nu\Psi\right)\left(\bar{\Delta}_\mu\gamma_\nu\Delta^\mu\bar{\Psi}\gamma^\nu\Psi\right)]\\&-\frac{\alpha_{TV}}{4}[\left(\bar{\Delta}_\mu\gamma_\nu\mathbf{T}\Delta^\mu\cdot\bar{\Psi}\gamma^\nu\boldsymbol{\tau}\Psi\right)\left(\bar{\Psi}\gamma_\nu\boldsymbol{\tau}\Psi\cdot\bar{\Psi}\gamma^\nu\boldsymbol{\tau}\Psi\right)\\&+\left(\bar{\Psi}\gamma_\nu\boldsymbol{\tau}\Psi\cdot\bar{\Delta}_\mu\gamma^\nu\mathbf{T}\Delta^\mu\right)\left(\bar{\Psi}\gamma_\nu\boldsymbol{\tau}\Psi\cdot\bar{\Psi}\gamma^\nu\boldsymbol{\tau}\Psi\right)\\&+\left(\bar{\Psi}\gamma_\nu\boldsymbol{\tau}\Psi\cdot\bar{\Psi}\gamma^\nu\boldsymbol{\tau}\Psi\right)\left(\bar{\Delta}_\mu\gamma_\nu\mathbf{T}\Delta^\mu\cdot\bar{\Psi}\gamma^\nu\boldsymbol{\tau}\Psi\right)\\&+\left(\bar{\Psi}\gamma_\nu\boldsymbol{\tau}\Psi\cdot\bar{\Psi}\gamma^\nu\boldsymbol{\tau}\Psi\right)\left(\bar{\Psi}\gamma_\nu\boldsymbol{\tau}\Psi\cdot\bar{\Delta}_\mu\gamma^\nu\mathbf{T}\Delta^\mu\right)]\\&-\eta_1[\left(\bar{\Delta}_\mu\Delta^\mu\right)\left(\bar{\Psi}\gamma_\nu\Psi\right)\left(\bar{\Psi}\gamma^\nu\Psi\right)\\&+\left(\bar{\Psi}\Psi\right)\left(\bar{\Delta}_\mu\gamma_\nu\Delta^\mu\right)\left(\bar{\Psi}\gamma^\nu\Psi\right)\\&+\left(\bar{\Psi}\Psi\right)\left(\bar{\Psi}\gamma_\nu\Psi\right)\left(\bar{\Delta}_\mu\gamma^\nu\Delta^\mu\right)]\\&-\eta_2[\left(\bar{\Delta}_\mu\Delta^\mu\right)\left(\bar{\Psi}\Psi\right)\left(\bar{\Psi}\gamma_\nu\Psi\right)\left(\bar{\Psi}\gamma^\nu\Psi\right)\\&+\left(\bar{\Psi}\Psi\right)\left(\bar{\Delta}_\mu\Delta^\mu\right)\left(\bar{\Psi}\gamma_\nu\Psi\right)\left(\bar{\Psi}\gamma^\nu\Psi\right)\\&+\left(\bar{\Psi}\Psi\right)\left(\bar{\Psi}\Psi\right)\left(\bar{\Delta}_\mu\gamma_\nu\Delta^\mu\right)\left(\bar{\Psi}\gamma^\nu\Psi\right)\\&+\left(\bar{\Psi}\Psi\right)\left(\bar{\Psi}\Psi\right)\left(\bar{\Psi}\gamma_\nu\Psi\right)\left(\bar{\Delta}_\mu\gamma^\nu\Delta^\mu\right)]\\&-\eta_3[\left(\bar{\Delta}_\mu\Delta^\mu\right)\left(\bar{\Psi}\gamma_\nu\boldsymbol{\tau}\Psi\right)\cdot\left(\bar{\Psi}\gamma^\nu\boldsymbol{\tau}\Psi\right)\\&+\left(\bar{\Psi}\Psi\right)\left(\bar{\Delta}_\mu\gamma_\nu\mathbf{T}\Delta^\mu\right)\cdot\left(\bar{\Psi}\gamma^\nu\boldsymbol{\tau}\Psi\right)\\&+\left(\bar{\Psi}\Psi\right)\left(\bar{\Psi}\gamma_\nu\boldsymbol{\tau}\Psi\right)\cdot\left(\bar{\Delta}_\mu\gamma^\nu\mathbf{T}\Delta^\mu\right)]\\&-\frac{f_{\pi NN}}{m_\pi}\left(\bar{\Delta}_\mu\gamma_\nu\gamma_5\boldsymbol{\tau}\Delta^\nu\right)\cdot\partial^\mu\left(\bar{\Psi}\gamma_5\boldsymbol{\tau}\Psi\right)\\&+\frac{g_{\pi N\Delta}}{m_\pi}\bar{\Delta}_\mu\mathcal{T}\cdot\Psi\partial^\mu\left(\bar{\Psi}\gamma_5\boldsymbol{\tau}\Psi\right)\\&+\frac{\mathrm{i}g_{\rho N\Delta}}{m_\rho}\bar{\Delta}_\mu\gamma_\nu\gamma_5\mathcal{T}\cdot\Psi\left(\partial^\nu(\bar{\Psi}\gamma_\mu\boldsymbol{\tau}\Psi)-\partial^\mu(\bar{\Psi}\gamma_\nu\boldsymbol{\tau}\Psi)\right)\\&+h.c.\end{aligned} \tag{A36}$$

The vector and scalar potentials can be expressed as

$$\begin{aligned}\Sigma_{i,PC}^0=&\alpha_V\rho+\alpha_{TV}\rho_3t_{3,i}+\gamma_{TV}\rho^3+\gamma_{TV}\rho_3^3t_{3,i}\\&+2(\eta_1+\eta_2\rho_s)\rho_s\rho+2\eta_3\rho_s\rho_3t_{3,i},\end{aligned} \tag{A37}$$

$$\begin{aligned}\Sigma_{i,PC}^S=&\alpha_S\rho_S+\beta_S\rho_s^2+\gamma_S\rho_s^3+\eta_1\rho^2+2\eta_2\rho_s\rho^2\\&+\eta_3\rho_3^2+\alpha_{TS}\rho_{s3}t_{3,i}.\end{aligned} \tag{A38}$$

The expressions for the symmetry energy and slope of the symmetry energy L for point-coupling RMF models are

$$\begin{aligned}S(\rho)_{PC}=&\frac{k_F^2}{6E_F^*}+\frac{1}{2}\alpha_V\rho+\eta_3\rho_s\rho\\&+\frac{1}{2}\alpha_{TS}\rho\left(\frac{m_N^{*2}}{E_F^{*2}[1-\alpha_{TS}A(\rho,m_N^*)]}\right),\end{aligned} \tag{A39}$$

$$
\begin{aligned}
L_{PC} = & \frac{k_F^2}{3E_F^*}\left(1-\frac{k_F^2}{2E_F^{*2}}-\frac{k_F^3 m_N^*}{E_F^{*2}\pi^2}\frac{\partial m_N^*}{\partial\rho}\right) \\
& +\frac{3}{2}\alpha_V\rho+3\eta_3\rho_s\rho+3\eta_3\rho^2\frac{\partial\rho_s}{\partial\rho} \\
& +\frac{1}{2}\alpha_{TS}\rho\left(\frac{m_N^{*2}}{E_F^{*2}[1-\alpha_{TS}A(\rho,m_N^*)]}\right) \\
& \times\left\{3-\frac{2k_F^2}{E_F^{*2}}+6\left(1-\frac{m_N^{*2}}{E_F^{*2}}\right)\frac{\rho}{m_N^*}\frac{\partial m_N^*}{\partial\rho}\right. \\
& +3\alpha_{TS}\frac{1}{1-\alpha_{TS}A}\left[2A\left(\frac{\rho}{m_N^*}\frac{\partial m_N^*}{\partial\rho}\right)\right. \\
& \left.\left.+\rho\frac{k_F^2}{E_F^{*3}}\left(1-3\frac{\rho}{m_N^*}\frac{\partial m_N^*}{\partial\rho}\right)\right]\right\}. \qquad \text{(A40)}
\end{aligned}
$$

APPENDIX B: IN-MEDIUM $NN \to N\Delta$ CROSS SECTION

By applying quasiparticle approximation [53], the in-medium cross sections are introduced via the replacement of the vacuum plane waves of the initial and final particles with the plane waves obtained by solving the nucleon and Δ equations of motion with scalar and vector fields. In detail, the matrix elements $\mathcal{M}^*$ for the inelastic scattering process $NN \to N\Delta$ are obtained by replacing the nucleon and Δ masses and momenta in free space with their effective masses and kinetic momenta [24], *i.e.*, $m \to m^*$ and $p^\mu \to p^{*\mu}$. As in Ref. [24], all calculations in this work are are performed for colliding nucleons with their center-of-mass frame coinciding with the nuclear matter rest frame.

The Feynmann diagrams corresponding to the inelastic-scattering $NN \to N\Delta$ processes are shown in Fig. B1, which include the direct and exchange processes. The $\mathcal{M}^*$-matrix derived from the interaction Lagrangian in Eq. (A3) can be written using the standard procedure [10]

$$
\mathcal{M}^* = \mathcal{M}_d^{*\pi} - \mathcal{M}_e^{*\pi} + \mathcal{M}_d^{*\rho} - \mathcal{M}_e^{*\rho}, \qquad \text{(B1)}
$$

where

$$
\begin{aligned}
\mathcal{M}_d^{*\pi} = & -\mathrm{i}\frac{g_{\pi NN}g_{\pi N\Delta}I_d}{m_\pi^2(Q_d^{*2}-m_\pi^2)}[\bar{\Psi}(p_3^*)\gamma_\mu\gamma_5 Q_d^{*\mu}\Psi(p_1^*)] \\
& \times[\bar{\Delta}_\nu(p_4^*)Q_d^{*\nu}\Psi(p_2^*)], \qquad \text{(B2)}
\end{aligned}
$$

$$
\begin{aligned}
\mathcal{M}_d^{*\rho} = & \mathrm{i}\frac{\Gamma_{\rho NN}g_{\rho N\Delta}I_d}{m_\rho}[\bar{\Psi}(p_3^*)\gamma_\mu\Psi(p_1^*)] \\
& \times\frac{g^{\mu\tau}-Q_d^{*\mu}Q_d^{*\tau}/m_\rho^2}{Q_d^{*2}-m_\rho^2} \\
& \times[\bar{\Delta}_\sigma(p_4^*)\gamma_\lambda\gamma_5(Q_d^{*\lambda}\delta_{\sigma\tau}-Q_d^{*\sigma}\delta_{\lambda\tau})\Psi(p_2^*)], \qquad \text{(B3)}
\end{aligned}
$$

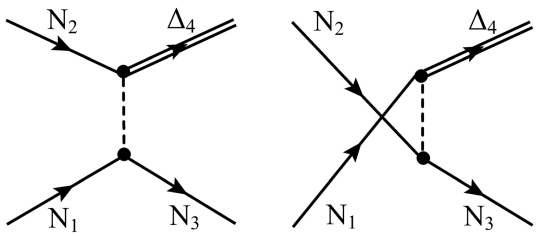

Fig. B1. Left diagram is the direct term and the right is the exchange term of the Feynmann diagram.

for the direct term, $Q_d^{*\mu} = p_3^{*\mu} - p_1^{*\mu}$, while the exchange term $\mathcal{M}_e^*$ is obtained by swapping $p_1^{*\mu} \longleftrightarrow p_2^{*\mu}$ and $Q_e^{*\mu} = p_3^{*\mu} - p_2^{*\mu}$. The isospin factors I_d, I_e are provided in Ref. [10].

The in-medium $NN \to N\Delta$ cross section is the averaged two-body cross section, considering the mass distribution of the Δ resonance as a short-lived state. It can be expressed as

$$
\sigma^*_{NN\to N\Delta} = \int_{m^*_{\Delta,\min}}^{m^*_{\Delta,\max}} \mathrm{d}m^*_\Delta f(m^*_\Delta)\tilde{\sigma}^*(m^*_\Delta), \qquad \text{(B4)}
$$

where $\tilde{\sigma}^*(m^*_\Delta)$ is the in-medium elementary two-body cross section. In the center-of-mass frame of colliding nucleons,

$$
\tilde{\sigma}^*(m^*_\Delta) = \frac{1}{64\pi^2}\int\frac{|\mathbf{p}^*_{\text{out, c.m.}}|}{\sqrt{s^*_{\text{in}}}\sqrt{s^*_{\text{out}}}|\mathbf{p}^*_{\text{in, c.m.}}|}\overline{|\mathcal{M}^*|^2}\mathrm{d}\Omega, \qquad \text{(B5)}
$$

where $\mathbf{p}^*_{\text{in, c.m.}}$ and $\mathbf{p}^*_{\text{out, c.m.}}$ are the momenta of incoming (1 and 2) and outgoing (3 and 4) particles, $s^*_{\text{in}} = (p_1^* + p_2^*)^2$, and $s^*_{\text{out}} = (p_3^* + p_4^*)^2$.

Here, $\overline{|\mathcal{M}^*|^2} = \frac{1}{(2s_1+1)(2s_2+1)}\sum_{s_1s_2s_3s_4}|\mathcal{M}^*|^2$ is

$$
\begin{aligned}
& \sum_{s_1s_2s_3s_4}|\mathcal{M}^*|^2 \\
= & \sum_{s_1s_2s_3s_4}\{|\mathcal{M}_d^{*\pi}|^2 - \mathcal{M}_d^{*\pi\dagger}\mathcal{M}_e^{*\pi} - \mathcal{M}_e^{*\pi\dagger}\mathcal{M}_d^{*\pi} + |\mathcal{M}_e^{*\pi}|^2 \\
& + |\mathcal{M}_d^{*\rho}|^2 - \mathcal{M}_d^{*\rho\dagger}\mathcal{M}_e^{*\rho} - \mathcal{M}_e^{*\rho\dagger}\mathcal{M}_d^{*\rho} + |\mathcal{M}_e^{*\rho}|^2 \\
& + \mathcal{M}_d^{*\pi\dagger}\mathcal{M}_d^{*\rho} - \mathcal{M}_d^{*\pi\dagger}\mathcal{M}_e^{*\rho} - \mathcal{M}_e^{*\pi\dagger}\mathcal{M}_d^{*\rho} + \mathcal{M}_e^{*\pi\dagger}\mathcal{M}_e^{*\rho} \\
& + \mathcal{M}_d^{*\rho\dagger}\mathcal{M}_d^{*\pi} - \mathcal{M}_d^{*\rho\dagger}\mathcal{M}_e^{*\pi} - \mathcal{M}_e^{*\rho\dagger}\mathcal{M}_d^{*\pi} + \mathcal{M}_e^{*\rho\dagger}\mathcal{M}_e^{*\pi}\}, \qquad \text{(B6)}
\end{aligned}
$$

where the $\mathcal{M}^*$-matrix is obtained from exchange by π and ρ mesons, and the detail calculations can be found in Ref. [27]. We show the calculation of $\sum_{s_1s_2s_3s_4}|\mathcal{M}_d^{*\pi}|^2$ as an example in the following:

$$\begin{aligned}
&\sum_{s_1 s_2 s_3 s_4} |\mathcal{M}_d^{*\pi}|^2 = \left(\frac{g_{\pi NN} g_{\pi N\Delta} I_d}{m_\pi^2 (Q_d^{*2} - m_\pi^2)}\right)^2 \\
&\times \sum_{s_1 s_2 s_3 s_4} [\Psi(p_1^*)\bar{\Psi}(p_1^*)\gamma_\mu\gamma_5 Q_d^{*\mu}\Psi(p_3^*)\bar{\Psi}(p_3^*)\gamma_\sigma\gamma_5 Q_d^{*\sigma}] \\
&\times [\Psi(p_2^*)\bar{\Psi}(p_2^*) Q_d^{*\nu}\Delta_\nu(p_4^*)\bar{\Delta}_\tau(p_4^*) Q_d^{*\tau}] \\
&= \left(\frac{g_{\pi NN} g_{\pi N\Delta} I_d}{m_\pi^2 (t^* - m_\pi^2)}\right)^2 \\
&\times \frac{2(m_{N_1}^* + m_{N_3}^*)^2((m_{N_1}^* - m_{N_3}^*)^2 - t^*)}{3 m_{\Delta_4}^{*2}} \\
&\times \left((m_{\Delta_4}^* - m_{N_2}^*)^2 - t^*\right)\left((m_{N_2}^* + m_{\Delta_4}^*)^2 - t^*\right)^2, \qquad \text{(B7)}
\end{aligned}$$

where $t = Q_d^{*2}$ for $|\mathcal{M}_e^{*\pi}|^2$ is $N_1 \longleftrightarrow N_2$. In Eq. (B5), the key element for the calculation of the cross section is the energy-momentum conservation in terms of the incoming ($p_{1,2}^\mu$) and outgoing ($p_{3,4}^\mu$) momenta of the particles. From the perspective of kinetic momentum, the energy-momentum conservation can be written as $p_1^\mu + p_2^\mu = p_3^\mu + p_4^\mu$ and can be expressed as $p_1^{*\mu} + \Sigma_1^{*\mu} + p_2^{*\mu} + \Sigma_2^{*\mu} = p_3^{*\mu} + \Sigma_3^{*\mu} + p_4^{*\mu} + \Sigma_4^{*\mu}$, $p_1^{*\mu} + p_2^{*\mu} = p_3^{*\mu} + p_4^{*\mu} - \Delta\Sigma^\mu$, where $\Delta\Sigma^\mu = \Sigma_1^\mu + \Sigma_2^\mu - \Sigma_3^\mu - \Sigma_4^\mu$ is the kinetic momentum change between the initial and final states. The change in effective energy is expressed as $\Delta\Sigma^0 = \Sigma_1^0 + \Sigma_2^0 - \Sigma_3^0 - \Sigma_4^0$, which is the same the formula as in Refs. [27, 54]. A similar issue exists in the calculation of $m_{\rm min}^*$, $m_{\rm max}^*$, and $\Gamma(m_\Delta^*)$, which are described in the following. Consequently, $p_1^{*0} + p_2^{*0}$ may differ from $p_3^{*0} + p_4^{*0}$, and $s_{\rm in}^* \neq s_{\rm out}^*$ in Eq. (B5), and they are related according to the following relationship:

$$\sqrt{s} = \sqrt{s_{\rm in}^*} + \Sigma_{N_1}^0 + \Sigma_{N_2}^0 = \sqrt{s_{\rm out}^*} + \Sigma_{N_3}^0 + \Sigma_{\Delta_4}^0. \qquad \text{(B8)}$$

This is derived from

$$\begin{aligned}
s &= (p_{N_1} + p_{N_2})^2 \\
&= (\sqrt{m_{N_1}^{*2} + \mathbf{p}_{N_1}^{*2}} + \sqrt{m_{N_2}^{*2} + \mathbf{p}_{N_2}^{*2}} + \Sigma_{N_1}^0 + \Sigma_{N_2}^0)^2 \\
&\quad - (\mathbf{p}_{N_1}^* + \mathbf{p}_{N_2}^*)^2 \\
&= (p_{N_3} + p_{\Delta_4})^2 \\
&= (\sqrt{m_{N_3}^{*2} + \mathbf{p}_{N_3}^{*2}} + \sqrt{m_{\Delta_4}^{*2} + \mathbf{p}_{\Delta_4}^{*2}} + \Sigma_{N_3}^0 + \Sigma_{\Delta_4}^0)^2 \\
&\quad - (\mathbf{p}_{N_3}^* + \mathbf{p}_{\Delta_4}^*)^2, \qquad \text{(B9)}
\end{aligned}$$

where $\mathbf{p}_{N_1}^* = -\mathbf{p}_{N_2}^*$ and $\mathbf{p}_{N_3}^* = -\mathbf{p}_{\Delta_4}^*$ in the center-of-mass frame.

The value of $m_{\Delta,\rm min}^*$ in the cross-section formula is determined by $\Delta \to N + \pi$ in isospin asymmetric nuclear matter, as in Refs. [27, 55], where both N and π are at rest. Additionally, the modification of the scalar and vector self-energies in this isospin exchange process must be taken into account. Thus,

$$m_{\Delta,\rm min}^* = m_N^* + m_\pi - \Delta\Sigma_d^0, \qquad \text{(B10)}$$

with $\Delta\Sigma_d^0 = \Sigma_\Delta^0 - \Sigma_N^0$. Here, $m_{\Delta,\rm max}^*$ is evaluated from $NN \to N\Delta$ for producing N and Δ at rest. This leads to

$$m_{\Delta,\rm max}^* = \sqrt{s} - m_{N_3}^* - \Sigma_{N_3}^0 - \Sigma_{\Delta_4}^0. \qquad \text{(B11)}$$

The in-medium Δ mass distribution $f(m_\Delta^*)$ is another crucial component of the in-medium $NN \to N\Delta$ cross section, for which proper energy conservation is also required, as $f(m_\Delta^*)$ is related to the $\Delta \to N + \pi$ process in isospin asymmetric nuclear matter. In this paper, the spectral function of Δ is obtained from Ref. [24]:

$$f(m_\Delta^*) = \frac{2}{\pi} \frac{m_\Delta^{*2}\Gamma(m_\Delta^*)}{(m_{0,\Delta}^{*2} - m_\Delta^{*2})^2 + m_\Delta^{*2}\Gamma^2(m_\Delta^*)}. \qquad \text{(B12)}$$

Here, $m_{0,\Delta}^*$ is the effective pole mass of Δ. The decay width $\Gamma(m_\Delta^*)$ is used in the parameterization form [24]

$$\Gamma(m_\Delta^*) = \Gamma_0 \frac{q^3(m_\Delta^*, m_N^*, m_\pi^*)}{q^3(m_{0,\Delta}^*, m_N^*, m_\pi^*)} \frac{q^3(m_{0,\Delta}^*, m_N^*, m_\pi^*) + \eta^2}{q^3(m_\Delta^*, m_N^*, m_\pi^*) + \eta^2} \frac{m_{0,\Delta}^*}{m_\Delta^*}, \qquad \text{(B13)}$$

where

$$q(m_\Delta^*, m_N^*, m_\pi^*) = \sqrt{\frac{\left((m_\Delta^* + \Sigma_\Delta^0 - \Sigma_N^0)^2 + m_N^{*2} - m_\pi^{*2}\right)^2}{4(m_\Delta^* + \Sigma_\Delta^0 - \Sigma_N^0)^2} - m_N^{*2}}. \qquad \text{(B14)}$$

The coefficients of Γ_0=0.118 GeV and η=0.2 GeV/c are used in the above parameterization formula.

The form factors are adopted to consider the contributions from high-order terms and the finite size of baryons [10, 56]:

$$F_N(t^*) = \frac{\Lambda_N^2}{\Lambda_N^2 - t^*} \exp\left(-b\sqrt{s^* - 4m_N^{*2}}\right), \qquad \text{(B15)}$$

$$F_\Delta(t^*) = \frac{\Lambda_\Delta^2}{\Lambda_\Delta^2 - t^*}. \qquad \text{(B16)}$$

Here, $F_N(t^*)$ is the form factor for nucleon-meson-nucleon coupling, and $F_\Delta(t^*)$ is that for nucleon-meson-Δ coupling, with b=0.046 GeV^{-1} for both ρNN and πNN coupling. The cutoff parameter $\Lambda_{\pi NN} \approx 1$ GeV, $\Lambda_{\rho NN}$, and $\Lambda_{\pi N\Delta}$ are determined by best fitting of the data of

$NN \to N\Delta$ cross section in free space ranging from $\sqrt{s}$=2.0 to 5 GeV [45]. Here, $\Lambda_{\rho N\Delta}$ is determined based on the relationship $\Lambda_{\rho N\Delta} = \Lambda_{\rho NN}\frac{\Lambda_{\pi N\Delta}}{\Lambda_{\pi NN}}$, as in [10]. Concerning the coupling constant $g_{\rho N\Delta}$, we use $g_{\rho N\Delta} \approx \frac{\sqrt{3}}{2}\Gamma_{\rho NN}\frac{m_\rho}{m_N}$, which is derived from the static quark model [10]. The cutoff parameters used in the calculations of the in-medium $NN \to N\Delta$ cross sections are listed in Table C1 in Appendix C.

APPENDIX C: PARAMETERS FOR DIFFERENT RMF MODELS

For the coupling constant parameters of $g_{m\Delta\Delta}$(where $m = \sigma, \omega, \rho, \delta$), we adopt $g_m = g_{m\Delta\Delta} = g_{mNN}$, consistent with the approach used in many studies involving transport models [11, 24, 26]. The parameters used in the effective Lagrangian are $g_{\pi NN}$=1.008, $g_{\pi N\Delta}$=2.202, m_π=138 MeV, m_N=939 MeV, and $m_{0,\Delta}$=1232 MeV.

Table C1. Saturation properties of all RMF models are used in this work. Except for m_N^*/m_N and $m_{0,\Delta}^*/m_{0,\Delta}$ in dimensionless units, and ρ_0 in fm^{-3}, all entries are in MeV. All $\Lambda_{\rho NN}$ = 1000 MeV, except for $\Lambda_{\rho NN}$ = 798, 650, and 580 MeV for FSUGOLD5, DDMEδ, and DDRH$_{\rho\delta}$.

Model	E_0	ρ_0	K_0	J	L	K_{sym}	m_N^*/m_N	$m_{0,\Delta}^*/m_{0,\Delta}$	$\Lambda_{\pi N\Delta}$
					Nonlinear models				
E [57]	−16.35	0.150	210.95	38.58	124.69	133.52	0.578	0.679	417
ER [57]	−16.25	0.149	215.91	39.41	126.63	128.12	0.582	0.682	416
NL1 [58]	−16.42	0.152	212.35	43.54	140.37	143.39	0.572	0.674	415
NL3 [59]	−16.24	0.148	269.91	37.34	118.32	100.53	0.596	0.692	417
NL3-II [59]	−16.26	0.149	270.62	37.67	119.57	103.19	0.593	0.690	417
NL3* [60]	−16.31	0.150	258.76	38.70	122.72	105.72	0.594	0.690	417
NL4 [61]	−16.16	0.148	273.33	36.34	115.31	100.41	0.595	0.692	417
NLC [62]	−15.77	0.148	221.76	35.23	108.52	76.14	0.633	0.720	417
NLB1 [58]	−15.80	0.162	276.73	32.94	102.12	75.61	0.621	0.711	420
NLB2 [58]	−15.80	0.162	239.96	32.93	110.57	157.15	0.557	0.662	421
NLRA1 [63]	−16.15	0.147	284.42	36.44	115.31	95.56	0.597	0.693	417
NLS [64]	−16.45	0.150	262.98	42.08	131.61	94.27	0.604	0.698	415
P-067 [65]	−16.31	0.160	245.72	41.80	124.81	48.93	0.665	0.745	416
P-070 [65]	−16.25	0.160	228.23	41.04	119.74	26.04	0.702	0.773	416
P-075 [65]	−16.51	0.170	253.33	42.17	119.16	−2.19	0.755	0.813	416
P-080 [65]	−15.84	0.160	251.71	39.28	108.78	−14.06	0.800	0.847	416
GL1 [66]	−16.30	0.153	200.08	32.50	94.68	33.08	0.700	0.772	418
GL2 [66]	−16.31	0.153	199.92	32.50	91.52	8.74	0.750	0.810	418
GL3 [66]	−16.31	0.153	199.87	32.50	89.03	−8.43	0.800	0.848	417
GL4 [66]	−16.31	0.153	249.88	32.50	94.31	25.23	0.700	0.772	418
GL5 [66]	−16.31	0.153	249.81	32.50	91.19	2.63	0.750	0.810	418
GL6 [66]	−16.31	0.153	249.90	32.50	88.73	−12.93	0.800	0.848	417
GL7 [66]	−16.30	0.153	299.99	32.50	93.94	17.94	0.700	0.772	418
GL8 [66]	−16.31	0.153	299.84	32.50	90.86	−2.91	0.750	0.810	418
GL82 [67]	−16.00	0.145	285.41	36.22	101.28	−8.06	0.773	0.827	416
GL9 [66]	−16.31	0.153	299.89	32.50	88.44	−16.84	0.800	0.848	417
GM1 [68]	−16.34	0.153	299.85	32.50	93.96	17.96	0.700	0.772	418
GM2 [68]	−16.31	0.153	299.94	32.50	89.34	−11.99	0.780	0.832	418
GM3 [68]	−16.30	0.153	239.93	32.50	89.71	−6.46	0.780	0.832	418
GPS1 [69]	−15.98	0.150	250.46	32.52	88.96	−12.54	0.800	0.848	417

Continued on next page

Table C1-continued from previous page

Model	E_0	ρ_0	K_0	J	L	K_{sym}	m_N^*/m_N	$m_{0,\Delta}^*/m_{0,\Delta}$	$\Lambda_{\pi N\Delta}$
GPS2 [69]	−15.96	0.150	300.67	32.52	88.66	−16.42	0.800	0.848	417
NLρA [29]	−16.00	0.160	240.16	30.34	84.52	3.38	0.750	0.809	419
NLρB [29]	−16.30	0.148	271.55	33.70	106.87	95.85	0.600	0.695	418
RMF301 [70]	−16.30	0.153	253.79	32.50	89.87	−6.24	0.775	0.829	418
RMF302 [70]	−16.30	0.153	249.64	32.50	89.65	−7.35	0.780	0.832	418
RMF303 [70]	−16.30	0.153	248.80	32.50	89.61	−7.57	0.781	0.833	418
RMF304 [70]	−16.30	0.153	247.97	32.50	89.57	−7.78	0.782	0.834	418
RMF305 [70]	−16.30	0.153	246.30	32.50	89.49	−8.21	0.784	0.835	418
RMF306 [70]	−16.30	0.153	244.62	32.50	89.40	−8.63	0.786	0.837	418
RMF307 [70]	−16.30	0.153	243.77	32.50	89.36	−8.83	0.787	0.838	418
RMF308 [70]	−16.30	0.153	242.94	32.50	89.32	−9.04	0.788	0.838	418
RMF309 [70]	−16.30	0.153	241.24	32.50	89.24	−9.45	0.790	0.840	418
RMF310 [70]	−16.30	0.153	238.68	32.50	89.12	−10.04	0.793	0.842	418
RMF311 [70]	−16.30	0.153	237.82	32.50	89.08	−10.24	0.794	0.843	417
RMF312 [70]	−16.30	0.153	236.96	32.50	89.04	−10.43	0.795	0.844	417
RMF313 [70]	−16.30	0.153	235.24	32.50	88.96	−10.82	0.797	0.845	417
RMF314 [70]	−16.30	0.153	234.39	32.50	88.92	−11.01	0.798	0.846	417
RMF315 [70]	−16.30	0.153	233.94	32.50	88.90	−11.10	0.799	0.846	417
RMF316 [70]	−16.30	0.153	233.51	32.50	88.88	−11.20	0.799	0.847	417
RMF317 [70]	−16.30	0.153	232.65	32.50	88.84	−11.38	0.800	0.848	417
RMF401 [70]	−16.31	0.153	229.87	32.50	93.78	23.04	0.710	0.779	418
RMF402 [70]	−16.31	0.153	231.87	32.50	93.77	22.74	0.710	0.779	418
RMF403 [70]	−16.31	0.153	229.88	32.50	93.12	18.06	0.720	0.787	418
RMF404 [70]	−16.47	0.153	230.42	32.50	93.14	17.86	0.720	0.786	418
RMF405 [70]	−16.31	0.153	233.88	32.50	93.09	17.50	0.720	0.787	418
RMF406 [70]	−16.31	0.153	233.92	32.50	89.75	−5.80	0.780	0.832	418
RMF407 [70]	−16.31	0.153	229.89	32.50	92.50	13.42	0.730	0.794	418
RMF408 [70]	−16.31	0.153	231.89	32.50	92.48	13.15	0.730	0.794	418
RMF409 [70]	−16.31	0.153	233.89	32.50	92.47	12.88	0.730	0.794	418
RMF410 [70]	−16.31	0.153	235.89	32.50	92.45	12.62	0.730	0.794	418
RMF411 [70]	−16.31	0.153	229.90	32.50	91.90	9.09	0.740	0.802	418
RMF412 [70]	−16.31	0.153	231.90	32.50	91.88	8.84	0.740	0.802	418
RMF413 [70]	−16.31	0.153	233.90	32.50	91.87	8.58	0.740	0.802	418
RMF414 [70]	−16.31	0.153	235.90	32.50	91.86	8.33	0.740	0.802	418
RMF415 [70]	−16.30	0.153	229.91	32.50	91.33	5.06	0.750	0.809	418
RMF416 [70]	−16.30	0.153	231.91	32.50	91.31	4.82	0.750	0.809	418
RMF417 [70]	−16.30	0.153	233.91	32.50	91.30	4.58	0.750	0.809	418
RMF418 [70]	−16.30	0.153	235.91	32.50	91.29	4.34	0.750	0.809	418
RMF419 [70]	−16.31	0.153	229.91	32.50	90.79	1.31	0.760	0.817	418
RMF420 [70]	−16.31	0.153	231.91	32.50	90.77	1.09	0.760	0.817	418
RMF421 [70]	−16.31	0.153	233.91	32.50	90.76	0.86	0.760	0.817	418

Continued on next page

Table C1-continued from previous page

Model	E_0	ρ_0	K_0	J	L	K_{sym}	m_N^*/m_N	$m_{0,\Delta}^*/m_{0,\Delta}$	$\Lambda_{\pi N\Delta}$
RMF422 [70]	−16.31	0.153	229.92	32.50	90.27	−2.17	0.770	0.825	418
RMF423 [70]	−16.31	0.153	231.91	32.50	90.26	−2.38	0.770	0.825	418
RMF424 [70]	−16.30	0.153	245.93	32.50	89.21	−9.88	0.790	0.840	418
RMF425 [70]	−16.30	0.153	247.94	32.50	89.20	−10.06	0.790	0.840	418
RMF426 [70]	−16.30	0.153	249.94	32.50	89.19	−10.24	0.790	0.840	418
RMF427 [70]	−16.30	0.153	235.94	32.50	88.83	−11.67	0.800	0.848	417
RMF428 [70]	−16.30	0.153	237.94	32.50	88.81	−11.85	0.800	0.848	417
RMF429 [70]	−16.30	0.153	239.94	32.50	88.80	−12.02	0.800	0.848	417
RMF430 [70]	−16.30	0.153	241.94	32.50	88.79	−12.19	0.800	0.848	417
RMF431 [70]	−16.30	0.153	243.94	32.50	88.78	−12.36	0.800	0.848	417
RMF432 [70]	−16.30	0.153	245.94	32.50	88.77	−12.53	0.800	0.848	417
RMF433 [70]	−16.30	0.153	247.94	32.50	88.75	−12.70	0.800	0.848	417
RMF434 [70]	−16.30	0.153	249.94	32.50	88.74	−12.87	0.800	0.848	417
Q1 [71]	−16.10	0.148	242.19	36.46	115.77	105.77	0.597	0.693	417
SMFT2 [72]	−13.85	0.162	210.02	17.37	52.72	60.28	0.656	0.738	430
S271 [38]	−16.24	0.148	270.94	35.03	101.91	22.28	0.700	0.771	417
SRK3M5 [73]	−16.00	0.150	299.95	23.50	82.46	146.79	0.550	0.657	425
DJM [72]	−14.81	0.172	245.71	20.23	63.03	32.62	0.569	0.671	430
HD [74]	−16.22	0.177	283.50	35.67	105.86	44.51	0.666	0.746	419
MS1 [75]	−15.75	0.148	249.97	35.00	106.76	38.56	0.600	0.695	418
MS3 [76]	−15.75	0.148	247.80	34.91	102.11	−0.10	0.601	0.696	418
NLSV1 [77]	−16.26	0.149	269.49	37.28	114.61	58.91	0.613	0.705	417
NLSV2 [77]	−16.24	0.147	293.95	36.84	111.78	39.60	0.618	0.709	417
TM1 [78]	−16.26	0.145	279.55	36.84	110.61	33.55	0.635	0.722	416
PK1 [79]	−16.22	0.148	283.39	37.61	115.78	55.17	0.605	0.700	417
Z271 [38]	−16.24	0.148	270.96	33.30	91.02	−16.40	0.800	0.848	417
hybrid [80]	−16.24	0.148	228.75	37.24	118.41	110.50	0.596	0.692	417
Z271* [81]	−16.24	0.148	268.69	40.18	83.52	−197.69	0.800	0.848	413
HC [74]	−15.75	0.169	233.88	31.06	58.60	−98.75	0.679	0.756	417
XS [76]	−16.30	0.148	228.11	31.78	54.85	−28.76	0.601	0.696	410
BKA20 [82]	−16.09	0.146	236.89	32.24	75.39	−15.04	0.642	0.727	412
BKA22 [82]	−16.08	0.147	223.09	33.13	78.67	−8.84	0.608	0.701	410
BKA24 [82]	−16.13	0.147	225.97	34.18	84.77	−14.95	0.603	0.698	413
FSUGOLD [83]	−16.28	0.148	228.56	32.54	60.38	−51.45	0.611	0.703	413
FSUGOLD4 [84]	−16.53	0.148	228.95	31.47	51.98	−16.12	0.610	0.703	410
FSUGOLD5 [84]	−16.92	0.148	229.53	30.56	45.66	23.28	0.610	0.703	413
FSUGZ00 [85]	−16.03	0.149	241.74	31.47	62.27	−3.22	0.605	0.699	410
FSUGZ03 [85]	−16.07	0.147	230.73	31.50	63.86	−11.75	0.603	0.698	410
FSUGZ06 [85]	−16.05	0.146	226.48	31.22	62.53	−24.49	0.607	0.700	410
IU-FSU [86]	−16.40	0.155	233.39	31.34	47.35	28.99	0.609	0.702	410
NL3V1 [87]	−16.24	0.148	269.60	36.01	101.08	0.62	0.596	0.692	416

Continued on next page

Table C1-continued from previous page

Model	E_0	ρ_0	K_0	J	L	K_{sym}	m_N^*/m_N	$m_{0,\Delta}^*/m_{0,\Delta}$	$\Lambda_{\pi N\Delta}$
NL3V2 [87]	−16.24	0.148	269.60	34.93	87.64	−46.25	0.596	0.692	416
NL3V3 [87]	−16.24	0.148	269.60	34.43	81.97	−56.29	0.596	0.692	416
NL3V4 [87]	−16.24	0.148	269.60	33.98	76.87	−60.12	0.596	0.692	415
NL3V5 [87]	−16.24	0.148	269.60	33.12	68.15	−53.40	0.596	0.692	415
NL3V6 [87]	−16.24	0.148	269.60	32.35	61.05	−34.30	0.596	0.692	414
S271V1 [87]	−16.24	0.148	270.98	35.73	95.92	−44.06	0.700	0.771	416
S271V2 [87]	−16.24	0.148	270.98	35.05	86.87	−90.33	0.700	0.771	416
S271V3 [87]	−16.24	0.148	270.98	34.42	78.86	−120.99	0.700	0.771	416
S271V4 [87]	−16.24	0.148	270.98	33.82	71.75	−139.52	0.700	0.771	415
S271V5 [87]	−16.24	0.148	270.98	33.27	65.44	−148.63	0.700	0.771	415
S271V6 [87]	−16.24	0.148	270.98	32.74	59.81	−150.45	0.700	0.771	415
Z271S1 [87]	−16.24	0.148	270.95	34.95	86.86	−64.86	0.800	0.848	415
Z271S2 [87]	−16.24	0.148	270.95	34.07	76.62	−92.28	0.800	0.848	415
Z271S3 [87]	−16.24	0.148	270.95	33.27	67.81	−104.57	0.800	0.848	414
Z271S4 [87]	−16.24	0.148	270.95	32.53	60.18	−106.04	0.800	0.848	414
Z271S5 [87]	−16.24	0.148	270.95	31.84	53.57	−99.82	0.800	0.848	413
Z271S6 [87]	−16.24	0.148	270.95	31.20	47.80	−88.22	0.800	0.848	412
Z271V1 [87]	−16.24	0.148	270.95	35.34	90.86	−66.36	0.800	0.848	416
Z271V2 [87]	−16.24	0.148	270.95	34.80	83.61	−104.83	0.800	0.848	416
Z271V3 [87]	−16.24	0.148	270.95	34.54	80.23	−120.38	0.800	0.848	415
Z271V4 [87]	−16.24	0.148	270.95	34.28	76.99	−133.75	0.800	0.848	415
Z271V5 [87]	−16.24	0.148	270.95	34.04	73.90	−145.14	0.800	0.848	415
Z271V6 [87]	−16.24	0.148	270.95	33.80	70.94	−154.73	0.800	0.848	415
G1 [71]	−16.14	0.153	215.34	38.51	123.30	97.03	0.633	0.721	417
G2 [71]	−16.07	0.154	215.00	36.40	100.71	−7.48	0.664	0.744	416
G2* [81]	−16.07	0.154	216.87	30.46	69.87	−21.86	0.663	0.743	413
TM1* [88]	−16.33	0.145	281.13	36.87	101.72	−13.78	0.634	0.721	415
BSR1 [89]	−16.02	0.148	239.60	31.03	59.39	12.92	0.605	0.699	410
BSR2 [89]	−16.03	0.149	241.81	31.54	62.14	−2.87	0.605	0.699	410
BSR3 [89]	−16.09	0.150	232.84	32.81	70.63	−7.45	0.604	0.698	410
BSR4 [89]	−16.08	0.150	236.47	33.12	73.09	−20.92	0.607	0.700	412
BSR5 [89]	−16.12	0.151	237.33	34.51	83.51	−14.00	0.607	0.700	413
BSR6 [89]	−16.13	0.149	233.88	35.57	85.54	−49.59	0.602	0.697	414
BSR7 [89]	−16.18	0.149	229.76	37.19	98.93	−17.04	0.602	0.697	415
BSR8 [89]	−16.04	0.147	231.44	31.09	60.29	−0.68	0.606	0.699	410
BSR9 [89]	−16.08	0.147	230.70	31.57	63.76	−11.42	0.603	0.698	410
BSR10 [89]	−16.07	0.147	224.90	32.65	70.64	−16.62	0.601	0.696	410
BSR11 [89]	−16.08	0.147	227.98	33.73	78.89	−24.71	0.605	0.699	412
BSR12 [89]	−16.10	0.147	230.14	33.93	77.73	−44.28	0.608	0.701	414
BSR13 [89]	−16.13	0.147	227.25	35.77	90.94	−41.62	0.604	0.698	415
BSR14 [89]	−16.18	0.147	233.29	36.24	93.64	−41.83	0.609	0.702	415

Continued on next page

Table C1-continued from previous page

Model	E_0	ρ_0	K_0	J	L	K_{sym}	m_N^*/m_N	$m_{0,\Delta}^*/m_{0,\Delta}$	$\Lambda_{\pi N\Delta}$
BSR15 [89]	−16.03	0.146	229.14	31.04	61.96	−21.36	0.607	0.700	410
BSR16 [89]	−16.05	0.146	226.57	31.29	62.45	−24.16	0.607	0.700	410
BSR17 [89]	−16.05	0.146	219.62	31.92	67.28	−31.57	0.609	0.702	410
BSR18 [89]	−16.05	0.146	221.63	32.76	72.69	−42.25	0.606	0.700	412
BSR19 [89]	−16.08	0.147	222.06	33.83	79.58	−50.19	0.608	0.701	414
BSR20 [89]	−16.09	0.146	222.69	34.51	87.97	−39.86	0.606	0.700	415
BSR21 [89]	−16.12	0.145	219.47	35.92	92.86	−45.94	0.602	0.697	415
SVI-1 [90]	−16.30	0.149	261.34	36.94	116.12	95.11	0.617	0.708	417
SVI-2 [90]	−16.31	0.149	273.61	37.13	116.39	91.95	0.620	0.710	417
SIG-OM [91]	−16.31	0.149	262.58	36.91	111.62	40.96	0.623	0.713	417
NL$\rho\delta$A [29]	−16.00	0.160	240.16	30.71	102.67	127.37	0.750	0.809	410
NL$\rho\delta$B [29]	−16.30	0.148	271.55	34.06	138.90	398.27	0.600	0.695	410
Density-dependent models									
DD-ME2 [52]	−16.14	0.152	251.27	32.31	51.27	−87.22	0.572	0.674	410
DD-ME1 [92]	−16.23	0.152	243.84	33.06	55.43	−101.03	0.578	0.678	410
TW99 [93]	−16.25	0.153	240.16	32.76	55.31	−124.69	0.555	0.661	412
DD-F [94]	−16.04	0.147	222.87	31.62	55.97	−139.71	0.556	0.662	413
DD2 [95]	−16.03	0.149	242.41	31.67	55.03	−93.21	0.563	0.667	412
DD [96]	−16.02	0.149	239.88	31.64	55.97	−95.29	0.565	0.668	412
PKDD [79]	−16.27	0.150	261.94	36.79	90.20	−80.54	0.571	0.673	415
DDMEδ [30]	−16.08	0.152	219.59	32.34	52.80	−118.13	0.609	0.702	416
DDRH$\rho\delta$ [31]	−16.25	0.153	240.16	25.09	47.81	81.15	0.555	0.661	417
Point-coupling models									
FA3 [50]	−16.02	0.152	275.90	29.69	29.08	−275.05	0.676	0.753	430
FA4 [50]	−16.09	0.152	293.79	29.77	30.65	−257.83	0.680	0.756	430
FZ3 [50]	−15.93	0.152	297.75	29.96	33.78	−262.69	0.742	0.803	430
VZ3 [50]	−16.04	0.148	282.09	34.03	121.49	151.25	0.626	0.715	430
PC-F1 [51]	−16.18	0.151	255.20	37.78	117.15	74.68	0.610	0.703	430
PC-F3 [51]	−16.18	0.151	254.99	38.26	118.57	74.74	0.610	0.703	430

References

[1] L. W. Chen, F. S. Zhang, X. H. Zeng *et al.*, Chin. Phys. C **22**, 1035 (1998)
[2] J. Y. Liu, W. J. Guo, S. J. Wang *et al.*, Phys. Rev. Lett. **86**, 975 (2001)
[3] Q. F. Li and Z. X. Li, Chin. Phys. Lett. **19**, 321 (2002)
[4] Y. X. Zhang and Z. X. Li, Phys. Rev. C **74**, 014602 (2006)
[5] Y. X. Zhang, Z. X. Li, and P. Danielewicz, ibid. **75**, 034615 (2007)
[6] G. Lehaut, D. Durand, O. Lopez *et al.*, Phys. Rev. Lett. **104**, 232701 (2010)
[7] O. Lopezet *et al.* (INDRA Collaboration), Phys. Rev. C **90**, 064602 (2014)
[8] L. W. Chen, F. S. Zhang, and Z. Y. Zhu, Phys. Rev. C **61**, 067601 (2000)
[9] Y. J. Wang, C. C. Guo, Q. F. Li *et al.*, Phys. Rev. C **94**, 024608 (2016)
[10] S. Huber and J. Aichelin, Nucl. Phys. A **573**, 587 (1994)
[11] T. Song and C. M. Ko, Phys. Rev. C **91**, 014901 (2015)
[12] J. Xu, L. W. Chen, M. B. Tsang *et al.*, Phys. Rev. C **93**, 044609 (2016)
[13] Y. Xun Zhang, Y. J. Wang, M. Colonna *et al.*, Phys. Rev. C **97**, 034625 (2018)
[14] A. Ono, J. Xu, M. Colonna *et al.*, Phys. Rev. C **100**, 044617 (2019)
[15] G. Jhang, J. Estee, J. Barney *et al.*, Phys. Lett. B **813**, 136016 (2021)
[16] H. Wolter, M. Colonna, D. Cozma *et al.*, PPNP **125**, 103962 (2022)
[17] M. Colonna, Y. X Zhang, Y. J. Wang *et al.*, Phys. Rev. C **104**, 024603 (2021)

[18] J. Xu, H. Wolter, M. Colonna *et al.*, Phys. Rev. C **109**, 044609 (2024)
[19] B. Haar and R. Malfliet, Phys. Rev. C **36**, 1611 (1987)
[20] B. Haar and R. Malfliet, Phys. Rep. **149**, 207 (1987)
[21] G. Mao, Z. Li, Y. Zhuo *et al.*, Phys. Rev. C **49**, 3137 (1994)
[22] G. J. Mao, Z. X. Li, Y. Z. Zhuo *et al.*, Phys. Lett. B **327**, 183 (1994)
[23] A. B. Larionov, W. Cassing, S. Leupold *et al.*, Nucl. Phys. A **696**, 747 (2001)
[24] A. Larionov and U. Mosel, Nucl. Phys. A **728**, 135 (2003)
[25] Q. F. Li, Z. X. Li, and G. J. Mao, Phys. Rev. C **62**, 014606 (2000)
[26] Q. Li and Z. Li, Phys. Lett. B **773**, 557 (2017)
[27] Y. Cui, Y. X. Zhang, and Z. X. Li, Phys. Rev. C **98**, 054605 (2018)
[28] Y. Cui, Y. X. Zhang, and Z. X. Li, Chin. Phys. C **43**, 024105 (2019)
[29] B. Liu, H. Guo, M. Di Toro *et al.*, Eur. Phys. J. A **25**, 293 (2005)
[30] X. Roca-Maza, X. Viñas, M. Centelles *et al.*, Phys. Rev. C **84**, 054309 (2011)
[31] T. Gaitanos, M. D. Toro, S. Typel *et al.*, Nucl. Phys. A **732**, 24 (2004)
[32] Y. Cui, Y. X. Zhang, Y. Tian *et al.*, Int. J. Mod. Phys. E **30**, 2150069 (2021)
[33] Y. Cui, Y. Tian, C. J. Xia *et al.*, NST **36**, 141 (2025)
[34] M. Dutra, O. Lourenço, S. S. Avancini *et al.*, Phys. Rev. C **90**, 055203 (2014)
[35] J. Piekarewicz, Phys. Rev. C. **66**, 034305 (2002)
[36] B. P. Abbott, R. Abbott, T. D. Abbott *et al.*, Phys. Rev. X **9**, 011001 (2019)
[37] M. C. Miller, F. K. Lamb, A. J. Dittmann *et al.*, Astrophys. J. Lett. **887**, L24 (2019)
[38] C. J. Horowitz and J. Piekarewicz, Phys. Rev. Lett. **86**, 5647 (2001)
[39] C. Ducoin, J. Marugueron, C. Providência *et al.*, Phys. Rev. C **83**, 045810 (2011)
[40] R. J. Furnstahl, Nucl. Phys. A **706**, 85 (2002)
[41] C. Ducoin, J. Margueron, and C. Providencia, Europhys. Lett. **91**, 32001 (2010)
[42] Z. Zhang and L.W. Chen, Phys. Lett. B **726**, 234 (2013)
[43] C. J. Horowitz, E. F. Brown, Y. Kim *et al.*, J. Phys. G **41**, 093001 (2014)
[44] M. D. Cozma, Phys. Rev. C **110**, 064911 (2024)
[45] A. Baldini, V. Flaminio, W. G. Moorhead *et al.*, Landolt-Börnstein, vol. **12** (Springer-Verlag, Berlin, 1987)
[46] J. Adamczewski-Musch, O. Arnold, C. Behnke *et al.*, EPJ A **56**, 259 (2020)
[47] M. Nan, P. C Li, G. J Wei *et al.*, arXiv: 2510.09337
[48] R. Machleidt, K. Holinde, and C. Elster, Phys. Rep. **149**, 1 (1987)
[49] M. Benmerrouche, R. M. Davidson, and N. C. Mukhopadhyay, Phys. Rev. C **39**, 2339 (1989)
[50] J. J. Rusnak and R. J. Furnstahl, Nucl. Phys. A **627**, 495 (1997)
[51] T. Bürvenich, D. G. Madland, J. A. Maruhn *et al.*, Phys. Rev. C **65**, 044308 (2002)
[52] G. A. Lalazissis, T. Nikšić, D. Vretenar *et al.*, Phys. Rev. C **71**, 024312 (2005)
[53] G. Baym and S. A. Chin, Nucl. Phys. A **262**, 527 (1976)
[54] Z. Zhang and C. M. Ko, Phys. Rev. C **97**, 014610 (2018)
[55] Z. Zhang and C. M. Ko, Phys. Rev. C **95**, 064604 (2017)
[56] T. Vetter, A. Engel, T. Bir *et al.*, Phys. Lett. B **263**, 153 (1991)
[57] M. Rufa, P. G. Reinhard, J. A. Maruhn *et al.*, Phys. Rev. C **38**, 390 (1988)
[58] P. G. Reinhard, Rep. Prog. Phys. **52**, 439 (1989)
[59] G. A. Lalazissis, J. Karatzikos, and P. Ring, Phys. Rev. C **55**, 540 (1997)
[60] G. A. Lalazissis S. Karatzikos, R. Fossion *et al.*, Phys. Lett. B **671**, 36 (2009)
[61] B. Nerlo-Pomoroska and J. Sykut, Int. J. Mod. Phys. E **13**, 75 (2004)
[62] B. D. Serot and J. D. Walecka, Int. J. Mod. Phys. E **6**, 515 (1997)
[63] M. Rashdan, Phys. Rev. C **63**, 044303 (2001)
[64] P. G. Reinhard, Z. Phys. A **329**, 257 (1988)
[65] A. Sulaksono, T. Mart, and C. Bahri, Phys. Rev. C **71**, 034312 (2005)
[66] N. K. Glendenning, *Compact Stars: Nuclear Physics, Particle Physics, and General Relativity*, 2nd ed. (Springer, New York, 2000)
[67] N. K. Glendenning, Phys. Lett. B **114**, 392 (1982)
[68] N. K. Glendenning and S. A.Moszkowski, Phys. Rev. Lett. **67**, 2414 (1991)
[69] S. K. Ghosh, S. C. Phatak, and P. K. Sahu, Z. Phys. A **352**, 457 (1995)
[70] A. A. Dadi, Phys. Rev. C **82**, 025203 (2010)
[71] R. J. Furnstahl, B. D. Serot, and H. B. Tang, Nucl. Phys. A **615**, 441 (1997)
[72] S. Gmuca, Z. Phys. A **342**, 387 (1992)
[73] M. Centelles, X. Vinas, M. Barranco *et al.*, Nucl. Phys. A **537**, 486 (1992)
[74] J. K. Bunta and S. Gmuca, Phys. Rev. C **68**, 054318 (2003)
[75] H. Müller and B. D. Serot, Phys. Rev. C **52**, 2072 (1995)
[76] F. J. Fattoyev and J. Piekarewicz, Phys. Rev. C **82**, 025805 (2010)
[77] M. M. Sharma, A. R. Farhan, and S. Mythili, Phys. Rev. C **61**, 054306 (2000)
[78] Y. Sugahara and H. Toki, Nucl. Phys. A **579**, 557 (1994)
[79] W. Long, J. Meng, N. VanGiai *et al.*, Phys. Rev. C **69**, 034319 (2004)
[80] J. Piekarewicz and M. Centelles, Phys. Rev. C **79**, 054311 (2009)
[81] A. Sulaksono and T. Mart, Phys. Rev. C **74**, 045806 (2006)
[82] B. K. Agrawal, Phys. Rev. C **81**, 034323 (2010)
[83] B. G. Todd-Rutel and J. Piekarewicz, Phys. Rev. Lett. **95**, 122501 (2005)
[84] J. Piekarewicz and S. P.Weppner, Nucl. Phys.A **778**, 10 (2006)
[85] R. Kumar, B. K. Agrawal, and S. K. Dhiman, Phys. Rev. C **74**, 034323 (2006)
[86] F. J. Fattoyev, C. J. Horowitz, J. Piekarewicz *et al.*, Phys. Rev. C **82**, 055803 (2010)
[87] C. J. Horowitz and J. Piekarewicz, Phys. Rev. C **66**, 055803 (2002)
[88] M. DelEstal, M. Centelles, X. Viñas *et al.*, Phys. Rev. C **63**, 024314 (2001)
[89] S. K. Dhiman, R. Kumar, and B. K. Agrawal, Phys. Rev. C **76**, 045801 (2007)
[90] M. M. Sharma, Phys. Lett. B **666**, 140 (2008)
[91] M. M. Haidari and M. M. Sharma, Nucl. Phys. A **803**, 159 (2008)
[92] T. Nikšić, D. Vretenar, P. Finelli *et al.*, Phys. Rev. C **66**, 024306 (2002)
[93] S. Typel and H. H. Wolter, Nucl. Phys. A **656**, 331 (1999)
[94] T. Klähn, D. Blaschke, S. Typel *et al.*, Phys. Rev. C **74**, 035802 (2006)
[95] S. Typel, G. Röpke, T. Klähn *et al.*, Phys. Rev. C **81**, 015803 (2010)
[96] S. Typel, Phys. Rev. C **71**, 064301 (2005)